The Mineralogy and Strength Characteristics of Selected Glaciolacustrine Clays in the Puget Sound Region

Andrew M. Gault

A report prepared in partial fulfillment of the requirements for the degree of

Master of Science
Earth and Space Sciences: Applied Geosciences

University of Washington

March, 2015

Project mentors:
Tom Badger, Washington State Department of Transportation
John LaManna, LaManna Geosciences, Inc.
Kathy Troost, Troost Geosciences, Inc.

Internship coordinator:
Kathy Troost

Reading Committee:
Alison Duvall
Juliet Crider

MESSAGe Technical Report Number: 019

Abstract

The combination of rainy climate, glaciolacustrine clays, and steep topography of the Puget Lowland creates slope stability issues for the regional population. Several glaciolacustrine deposits of laminated silt and clay of different ages contribute to the likelihood of slope failure. The glaciolacustrine deposits are generally wet, range in thickness from absent to >30m, and consist of laminated silt and clay with sand interbeds at the tops and bottoms, sandy laminae throughout the deposits, occasional dropstones and shear zones. The glaciolacustrine deposits destabilize slopes by 1) impeding groundwater flow percolating through overlying glacial outwash sediments, 2) having sandy laminae that lower strength by increasing pore pressure during wet seasons, and 3) increasing the potential for block-style failure because of secondary groundwater pathways such as laminae and vertical fractures. Eight clay samples from six known landslide deposits were analyzed in this study for their mineralogy, clay fraction and strength characteristics. The mineralogy was determined using X-ray Diffractometry (XRD) which revealed an identical mineralogic suite among all eight samples consisting of chlorite, illite and smectite. Nonclay minerals appearing in the X-ray diffractogram include amphibole and plagioclase after removal of abundant quartz grains. Hydrometer tests yielded clay-size fraction percentages of the samples ranging from 10% to 90%, and ring shear tests showed that the angle of residual shear resistance (ϕ_r) ranged from 11° to 31°. Atterberg limits of the samples were found to have liquid limits ranging from 33 to 83, with plastic limits ranging from 25 to 35 and plasticity indices ranging from 6 to 48. The results of the hydrometer and residual shear strength tests suggest that ϕ_r varies inversely with the clay-size fraction, but that this relationship was not consistent among all eight samples. The nature of the XRD analysis only revealed the identity of the clay minerals present in the samples, and provided no quantitative information. Thus, the extent to which the mineralogy influenced the strength variability among the samples can't be determined given that the mineral assemblages are identical. Additional samples from different locations within each deposit along with quantitative compositional analyses would be necessary to properly account for the observed strength variability.

Table of Contents

Acknowledgements vi
1.0 Introduction 1
1.1 Geologic Setting 2
1.2 Study Area 3
1.2.2 Ledgewood Slide 3
1.2.3 Woodway Slide 4
1.2.4 Discovery Park 4
1.2.5 SR-520 Slope Failure 4
1.2.6 Klickitat Drive Slope Failure 5
1.3 Scope of Work 5
2.0 Methods 5
2.1 XRD 5
2.1.1 XRD Background 5
2.1.2 Sample Preparation for XRD 7
2.2 Atterberg Limit Tests 9
2.3 Residual Shear Strength 9
2.4 Hydrometer Tests 10
3.0 Results 11
4.0 Discussion 12
5.0 Conclusion 13
Appendix – Data Descriptions 38
A.1 Oso Landslide 38
A.2 Ledgewood Slide 40
A.3 Woodway Slide 42
A.4 Discovery Park 44
A.5 SR-520 Shaft 7 46
A.6 SR-520 Shaft 18 48
A.7 SR-520 Shaft 21 50
A.8 Klickitat Drive 52

List of Figures

Figure 1 18
Figure 2 19
Figure 3 20
Figure 4 21
Figure 5 22
Figure 6 23
Figure 7 24
Figure 8 25
Figure 9 26
Figure 10 27
Figure 11 28
Figure 12 29
Figure 13 30
Figure 14 31
Figure 15 32
Figure 16 33
Figure 17 34
Figure 18 35
Figure 19 39
Figure 20 41
Figure 21 43
Figure 22 45
Figure 23 47
Figure 24 49
Figure 25 51
Figure 26 53

List of Tables

Table 1 36
Table 2 37

Acknowledgements

I am indebted to the Washington State Department of Transportation (WSDOT) for providing the financial assistance that made this project possible. Thanks are due to Mr. Samuel Wade at WSDOT for his training on the ring shear testing apparatus and on performing the hydrometer tests. Thanks also go to Mr. Jeff Taylor at WSDOT for his coaching on hydrometer test sample preparation and for allowing me to use the high temperature oven. I would like to thank Mr. Robert Grandorff at WSDOT for supplying some of the clay samples analyzed in this project along with the associated lab data. My gratitude also goes to Mr. Tony Allen at WSDOT for allowing me access to information on the SR-520 project.

At the University of Washington, I would like to thank Ms. Kathy Troost for her mentorship and for sharing her vast knowledge of Puget Sound geology, suggesting this project, for providing me her laboratory in which to do this work, and for the time she spent keeping me on course throughout this project. Thanks go to Dr. Alison Duvall and Dr. Juliet Crider for reading my draft submissions and giving me thought-provoking feedback and revision suggestions. I would also like to Ms. Tuesday Kuykendall and her assistant, Ms. Tatyana Galenko of the Materials Science and Engineering User Facility. Their education on the concept of X-ray Diffractometry and training on using the X-ray Diffractometer were valuable to my success in obtaining X-ray diffraction patterns.

I would like to thank Mr. Sean Cool and Mr. Gordon Denby of GeoEngineers, Inc., Dr. Richard Finno of Northwestern University, Dr. Robert D. Holz, Professor Emeritus of the University of Washington, and Dr. Timothy D. Stark of the University of Illinois at Urbana-Champaign for their interest in this project at its outset. Each of their recommendations and advice were invaluable for me to get this project started in the right direction.

Finally, my gratitude goes to Mr. John LaManna of LaManna Geosciences, Inc., and to Mr. Tom Badger of WSDOT. I truly appreciate the mentorship, enthusiasm and support they provided me from the beginning of this project all the way through to the end. This project would not have been possible without their guidance.

1.0 Introduction

The hilly topography that is characteristic of the Puget Lowland largely represents the legacy of continental glaciation that occurred in the Puget Sound region over the last 2.4 Ma (Troost and Booth, 2008). Glacial sediments of variable thickness covers the ridges and glacially carved troughs of the Puget Lowland; features that provide testament to the power of moving ice to carve landscapes by grinding, transporting and depositing rock debris (Savage et al., 2000). The glacial deposits consist of fine-grained glaciolacustrine sediments that are overconsolidated as a result of having been overridden by glaciers and subjected to the weight of thousands of feet of ice, and are therefore very dense and hard. The glaciolacustrine sediments underlie coarse-grained outwash sediments that are capped incompletely with a layer of glacial till, then by recessional outwash. (Troost and Booth, 2008). These sediments and post-glacial fill are thickest in the glacially carved troughs and now supports the infrastructure of the densely-populated greater Seattle area and its surrounding counties (Troost and Booth, 2008). Gravity acting on steep slopes, elevated groundwater levels during storm events and extensive alteration from development, act to destabilize the post-glacial sediments which results in common slope failures (Savage et al., 2000). Moreover, the contact between glaciolacustrine and overlying coarser-grained deposits is frequently associated with slope failure throughout the Puget Lowland (Savage et al., 2000). Stormwater percolating through the permeable coarse sediments pools on the low permeability surface of the clay-rich layer, causing destabilization by elevating pore pressure in the overlying sediments and creating a slide plane on the fine-grained surface (Tubbs, 1974).

The terms *clay* and *clay mineral* are distinct from one another in that *clay* is a general term used to describe a sedimentary rock of a grain size <2 μm, whereas *clay mineral* refers to a specific layered hydrous aluminosilicate (Moore and Reynolds, 1997). Examples of common clay mineral groups include illite, smectite and chlorite (West, 1995). Members of the illite and smectite groups have a three-layer sequence of tetrahedral sheets (t) sandwiching an octahedral sheet (o) in their repeating structural units (t-o-t). Chlorite has a mixed-layer repeating structure of a t-o-t layer separated by a single o-sheet (West, 1995). Minerals of the three-layer structure category are susceptible to shrinking and swelling in the presence of water. The most problematic of these minerals are those of the smectite group in which their capacity to expand and contract reduces the strength of deposit, thereby affecting slope stability (Borchardt, 1977).

To better understand the engineering behavior of clay-rich deposits, the mineralogy and strength characteristics of the clays need to be determined. Prior studies have identified the mineralogy of some of the Puget Lowland glaciolacustrine deposits (e.g. Mullineaux, 1967; Subbarao, 1953), though these studies are few in number. Mullineaux determined that these deposits have a homogeneous mixture if illite, chlorite and montmorillonite, where montmorillonite is a member of the smectite clay mineral group. Subbarao conducted an in depth investigation of the glaciolacustrine Superior Clay using several approaches to mineralogic analysis and found that the clay contained illite, chlorite, montmorillonite, kaolinite, and numerous non-clay minerals.

The approach of this study is different from the previous study examples in that it focuses on determining the mineralogy and the strength characteristics of clays associated with known slope failure deposits. The goals are to determine what correlation exists between the mineralogy and the residual shear strength of the clays, and to contribute data on strength parameters that could be used to inform geotechnical studies on these landslide deposits (Figure 1). This work is important because of the limited information available of this nature on the glaciolacustrine deposits of the Puget Sound region, and for safeguarding the public from loss of life because of related slope failures.

1.1 Geologic Setting

During the Pleistocene the Puget Lowland experienced repeated advance and retreat of continental ice sheets. These ice sheets deposited units of fine-grained glaciolacustrine deposits, which exist in the Puget Lowland as bedded silt and clay deposits of varying ages which are overlain by loosely consolidated proglacial outwash. This sequence of glacial deposits is common in the subsurface and in bluff exposures. The ages of these sediment packages are often unknown because of a lack in absolute dating and a lack of distinguishing characteristics. The youngest of these are the glaciolacustrine clays deposited by the Vashon glacier, which receded northward approximately 16,400 years ago (Troost and Booth, 2008). These clay-rich deposits formed as streams delivered fine-grained sediment into the still-water environments of proglacial lakes (Mullineaux et al., 1965). As the Vashon glacier advanced southward, meltwater streams laid down the Esperance Sand in front of the glacier, which is a large unit of coarse-grained alluvium deposited on top of a glaciolacustrine deposit known as the Lawton Clay (Mullineaux et al., 1967). At the top of the glacial sequence, an extensive but discontinuous layer of glacial

till caps the Esperance Sand, and marks the arrival of the Vashon glacier (Troost and Booth, 2008).

1.2 Study Area

A total of eight fine-grained soil samples from six separate slope failure deposits were analyzed in this project. This section provides brief descriptions of the sample deposits and their geographic locations. From north to south, these are the Oso landslide, the Ledgewood landslide, the Woodway landslide, the Discovery Park sampling point, the SR-520 slope failure, and the Klickitat Drive slope failure. These sample locations are contained in an area that covers a 20 km-wide swath of the Puget Lowland that stretches from south of Seattle approximately 20 km to about 80 km north of Seattle (Figure 1). Three samples identified as Shaft 7, Shaft 18 and Shaft 21 came from the SR-520 slope failure.

1.2.1 Oso Landslide

The Oso landslide occurred on March 22, 2014 on the slope of the Whitman Bench above the North Fork of the Stillaguamish River near the town of Oso, WA following a period of higher than normal precipitation during February and March (Robertson, 2014) (Figure 2). Over 7 million cubic meters of material moved during the event with the slide runout extending over one kilometer (Robertson, 2014). The glaciolacustrine unit is mapped as advance glaciolacustrine deposits of Vashon age (Dragovich, et al., 2003). WSDOT provided the clay sample from this slope failure from near the base of the slope.

1.2.2 Ledgewood Slide

The Ledgewood slide occurred on March 27, 2013 on a coastal bluff of Whidbey Island along Puget Sound above Ledgewood Beach southeast of Coupeville, WA (Gordon and Cool, 2013) (Figure 3). The Ledgewood slide represents the most recent movement of the Driftwood Way landslide that has experienced intermittent activity over several decades. (Gordon and Cool, 2013). Based on stratigraphic relationships, this glaciolacustrine deposit appears to be of pre-Vashon age and exhibited extensive deformation, shearing and slickensides (Kathy Troost, verbal communication, March 2015). University of Washington Geologist Kathy Troost

provided the sample for this slide, which came from clay exposed in the toe of the slide on Ledgewood Beach (Figure 4).

1.2.3 Woodway Slide

The Woodway slide occurred on January 17, 1997 on a coastal bluff along Puget Sound in the town of Woodway, WA (Figure 5). On this date, an estimated 75,000-150,000 cubic meters of glacial sediments slid down the steep bluff south of Deer Creek, pushing several cars of a passing freight train into Puget Sound (Baum et al., 1998). Based on stratigraphic relationships, this clay sample appears to be from the Lawton Clay (Kathy Troost, verbal communication, March 2015). I collected the sample for this slide from bedded clay exposed in the failure deposit.

1.2.4 Discovery Park

The type sequence of proglacial Vashon deposits is exposed in the south bluff in Discovery Park in Seattle, WA. The glaciolacustrine clay exposed in the middle of the bluff is known as the Lawton Clay (Figure 6) (Mullineaux et al., 1965). The Discovery Park sample is not associated with a specific landslide deposit, though small scale failures frequently occur in the south bluff at this location. I collected the sample from sluffed blocks of clay that had eroded from this unit that were accessible at the bluff base.

1.2.5 SR-520 Slope Failure

A slope failure occurred On November 28, 2011 next to the eastbound lanes of SR-520 in Bellevue, WA following a slope grading excavation below the off-ramp to Bellevue Way. The toe of the slope was excavated to allow construction of an access road parallel to the eastbound lanes to facilitate widening of SR-520 as part of a floating bridge replacement project (Stark, 2013) (Figure 7). After a 20-foot wide excavation exposed glaciolacustrine clay at the toe of the slope, the action of unloading the clay produced tension cracks that allowed water to infiltrate and decrease the clay strength (Stark, 2013). The tension cracks progressed into a landslide occurring on November 28, 2011 (Stark, 2013). The clay deposit may be from a pre-Vashon glaciation (Kathy Troost, verbal communication, March 2015). WSDOT provided the three samples Shaft 7, Shaft 18 and Shaft 21 from this slope failure.

1.2.6 Klickitat Drive Slope Failure

A shallow landslide occurred in March 2014 on the slope above Klickitat Drive near the interchange of I-5 and SR 518 in Tukwila, WA (Bartoy, 2014). The 2014 failure extended about 30 m to 50 m downslope, and exposed about 1.5 m of the head scarp at the top of the slope approximately 75 m wide (Bartoy, 2014). The slope failure occurred after heavy rains saturated soil that was part of a larger landslide that had failed during the construction of I-5 in the 1960's (Bartoy, 2014). This sample may have come from Vashon glaciolacustrine recessional sediments (Kathy Troost, verbal communication, March 2015). WSDOT provided the clay sample from this slope failure.

1.3 Scope of Work

The goals of this study were to 1) determine the mineral composition of glaciolacustrine clays associated with known landslide deposits, 2) see whether a correlation exists between the mineralogy and the residual shear strength, and 3) contribute data on strength properties of these clays. I used X-ray diffraction (XRD) to determine the mineralogy of the clay, Atterberg limit tests to determine the clay liquid limits (LL) and plastic limits (PL), ring shear tests to determine the angle of residual shear strength (ϕ_r), and hydrometer tests to determine the sample clay fractions (CF). CF is defined as the percentage of particles finer than 2μm.

2.0 Methods

This section describes how the clay samples were prepared and analyzed using X-ray Diffraction (XRD), and how the samples were tested for their Atterberg limits, residual shear strength and CF.

2.1 XRD

2.1.1 XRD Background

Clay minerals form in low temperature environments near the Earth's surface from the interaction of water with weathered rock minerals and poorly crystallized substances such as volcanic glass. This interaction allows for greater structural complexity than those of minerals crystallizing at higher temperatures (Perkins, 2002). The intricacy and small size of clay

minerals requires laboratory techniques and analysis with XRD as an aid for differentiating between clay mineral species (Poppe et al., 2001).

Clay minerals have a platy structure in which their atoms are organized in a repeating pattern arranged on planes that are separated by equal distances (Moore and Reynolds, 1997) (Figure 8). X-rays striking the atoms in the planes are diffracted. The diffracted X-rays scatter and interfere with one another either constructively or destructively. Destructive interference occurs when the diffracted X-ray waves are out of phase with one another, and thus combine to partially or completely cancel the energy of the resultant X-ray. Constructive interference occurs when the waves of the scattered X-rays are completely in phase with one another, and thus combine to produce a resultant X-ray of increased energy (Moore and Reynolds, 1997). The constructively diffracted X-rays emanate from the crystal structure at angles that are unique to each mineral (Figure 8).

An X-ray Diffractometer is a device used to generate X-rays and measure the angle and intensity of diffracted rays as a means of identifying the composition of materials consisting of minute particles (Pei-Yuan, 1977). The diffractometer focuses X-rays onto the surface of a clay sample, and the detector measures the intensity and the angle of diffracted X-rays striking the detector. Diffracted waves must be of sufficient energy to be recorded by the detecting device of an X-ray Diffractometer (Figure 9). The detector measures the intensity in "counts" of the number of X-ray photons striking the detector per second, and the goniometer measures the diffraction angle in degrees 2θ as the machine rotates the detector through a preset 2θ range. JADE XRD software connected to the diffractometer produces a plot of the diffraction angle versus the intensity of the diffracted beam on a graph known as a diffractogram (Figure 10).

The minerals present in a sample diffract X-rays at angles 2θ specific to each mineral, producing diffraction peaks in the diffractogram at unique 2θ angles (Moore and Reynolds, 1997). Most clay minerals will produce multiple diffraction peaks at evenly spaced angles along the 2θ axis. The multiple diffraction peaks that the minerals produce are known as diffraction peak orders. The distances between the diffraction peak orders along the 2θ axis are the same for a given mineral (Moore and Reynolds, 1997). For example, the distance between the first order diffraction peak for chlorite (001) and the second order diffraction peak for chlorite (002) will be the same as the distance between 002 and the third order diffraction peak (003), and so on (Figure 10).

The heights of the peaks (a function of the number diffracted X-rays striking the detector) can vary from sample to sample depending on factors such as sample thickness, but the ratio between the heights of the peaks between diffraction orders will remain essentially constant. For example, the height of the chlorite 002 peak may be taller in a diffractogram for a given sample of certain clay than in a diffractogram of a second sample of the same clay, the thickness of which happened to be less than the first. However, the chlorite 002/003 height ratio of approximately 1 to 4 is a characteristic of the clay mineral and will not change from sample to sample (Figure 10).

Each mineral present in a sample can be identified based on the unique pattern of diffraction peaks the mineral produces, though some clay minerals produce peaks at angles close enough to coincide on the pattern. In these instances, the property that clay minerals may expand, contract, or collapse in response to different chemical and physical treatments can be used to help confirm or eliminate the presence of such minerals (Moore and Reynolds, 1997). These responses show up in the diffractograms as changes in peak intensity and shifts in peak location along the 2θ axis. In this study, the chemical treatments included saturating the samples with solutions of magnesium chloride and potassium chloride, and exposing the samples to the vapors of ethylene glycol and glycerol (solvation). The physical treatments included air drying, heating to 300 °C, and heating to 550 °C. How these treatments were applied is discussed in the following section on sample preparation for XRD. In this study, I identified the clay mineralogy by matching the 2θ peak data of the diffractogram patterns to published diffraction data for the minerals. In addition, I compared the effects that the heat and chemical treatments produced on the diffractograms to published results expected for these treatments as a guide for confirming the presence of specific minerals (Moore and Reynolds, 1997).

2.1.2 Sample Preparation for XRD

Preparing the clay samples for XRD analysis takes place in two steps. The first step is to isolate the <2μm sediment size fraction. This step removes most of the non-clay minerals. The second step is use preferred orientation. This step enhances the basal diffraction peaks and allows for better detection of the clay responses to the various treatments. Forcing the clay minerals into this preferred orientation also greatly simplifies the diffractogram by filtering out the influence of the a- and b-crystallographic axes, which are nearly equal among the many clay

minerals. This process leaves the c-crystallographic axes presented to the X-ray beam, and thus allows the signature peaks of the clay minerals to clearly stand out for easy identification (Moore and Reynolds, 1997).

I developed the preferred mineral orientations in a process of several steps. In the first step of this process, approximately 25 grams of sample is crushed with a mortar and pestle, placed in a beaker with 400 ml of deionized water, and then disaggregated for five minutes using an ultrasonic cleaner. This is necessary to prevent the suspended clay particles from flocculating, or clumping back together (Poppe et al., 2001). In the second step, the <2 μm fraction is separated from the larger-sized particles by centrifuging the disaggregated clay at 800 RPM for approximately 4 minutes. This step suspends the <2 μm fraction so that these sediments can be captured by vacuum filtration, thus forcing the platy minerals to lie flat on a 0.45 μm filter disc. The filter cake is transferred to a glass petrographic slide by holding the filter taught around the outside of a glass cylinder and "rolling" the cake onto the slide. The filter cake binds to the slide with the platy clay minerals lying flat so that the c-crystallographic axes are oriented perpendicular to the glass slide surface.

To evaluate of diagnostic response of clays to various treatments, I created four slides for each of the eight clay samples. As mentioned in section 2.2, these treatments included air-drying, saturation with magnesium ions and potassium ions, heating to 300 °C, heating to 550 °C, and solvation with glycerol and ethylene glycol. Saturating the samples with magnesium and potassium ions places uniform cations in the cation exchange positions of the clay mineral structures. For the saturation treatments, I saturated three of the four slides during the suction filtration step with approximately 3 ml of 0.1M magnesium chloride solution (Mg). I saturated the fourth slide during filtration with ~3 ml of 1M potassium chloride (K). Of the three Mg-saturated slides, one slide was X-rayed three times; once under its air-dried condition (Mg-AD), again after being heated to 300 °C for one hour (Mg-300), and for a last time after being heated to 550 °C for one hour (Mg-550). Of the two remaining Mg-saturated slides, one was X-rayed after being solvated in ethylene glycol vapors (Mg-glycol), and the other was X-rayed after being solvated in glycerol vapors (Mg-glycerol) (Moore and Reynolds, 1997). Finally, the K-saturated slide was X-rayed under its air-dried condition (K-AD), and then again after being heated to 300 °C for one hour (K-300) (Moore and Reynolds, 1997).

2.2 Atterberg Limit Tests

Atterberg limits are measurements of fine-grained soil consistency based on the moisture content of the soil. The two common limits used in geotechnical engineering are the liquid limit (LL) and the plastic limit (PL) (Reddy, 2002). The PL is the moisture content that defines the point at which the soil changes from semi-solid to a plastic (flexible) state. The LL is the moisture content marking the point at which a soil changes from a plastic state to a viscous fluid state (Reddy, 2002). The plasticity index (PI) is the difference between LL and the PL values and represents the range of moisture contents at which the soil exhibits plasticity. The technical definition for LL is the moisture content, in percent, at which two halves of a soil cake will flow together, for a distance of 12.7 mm along the bottom of a groove of standard dimensions separating the two halves, when the cup of a standard LL apparatus is dropped 25 times at a rate of two drops per second from a height of 10 mm (NYDOT, 2007) (Figure 11). The PL is defined as the moisture content, in percent, at which a soil will just begin to crumble when rolled into a thread 3 mm in diameter on a ground glass plate (NYDOT, 2007).

The American Standards of Testing and Materials (ASTM) covers the procedure for determining the Atterberg limits in ASTM standard D4318-10: Standard Test Methods for Liquid Limit, Plastic Limit, and Plasticity Index of Soils (ASTM, 2010). I performed Atterberg limits at the UW campus following the methods described in standard D4318-10 on the Ledgewood, Woodway and Discovery Park samples. I also sent portions of these same three samples to WSDOT for them to duplicate Atterberg limits as a check on my results. For the LL test, standard D4318- 10 outlines two testing methods: the three point method, and the single point method. At UW, I used the three point method to determine LL for the Ledgewood, Woodway, and Discovery Park samples. Later, I discovered that the WSDOT standard procedure is the single-point method. Since WSDOT had previously conducted Atterberg limits on the Klickitat, Oso, and the three SR-520 samples, for consistency I use the LL, PL and PI values from WSDOT for all eight of the samples in this study. The convention for reporting the LL, PL and PI values is to omit the percent sign (ASTM, 2010), and is the reporting method I use here.

2.3 Residual Shear Strength

Clays have a limit to the amount of shear stress that they can withstand before failing. This limit is known as the peak shear strength, which is a measure of the maximum resistance

clay has to shear stress, or forces acting laterally on the clay. When clay is exposed to increasing shear stress, the peak resistance to the shear force will eventually be exceeded, and the clay goes into a slightly lower but steady shear resistance known as the residual shear strength (Stark and Hussein, 2013).

To evaluate the residual shear strength of the samples, I conducted ring shear tests following the procedure given in ASTM standard D6467-13: Standard Test Method for Torsional Ring Shear Test to Determine Drained Residual Shear Strength of Cohesive Soils (ASTM, 2013). This ring shear test takes place in two phases. In the first phase, or consolidation phase, a clay sample is placed in the ring-shaped recess of a sample vessel and consolidated at five steps (A, B, C, D, and E) at progressively higher normal stress (Table 1). Following the consolidation phase, the clay is then sheared during the shearing phase in another five steps under the same progressively higher normal shear stress loads. The device used to perform the residual strength tests on the clays is the Wykeham Farrance "Torshear" Anular Ring Shear Tester located at the WSDOT State Materials Testing Laboratory in Tumwater, WA (Figure 12).

Because this ring shear tester was available for a limited time period, it was decided that five of the eight samples would be tested. WSDOT already conducted testing on the Oso and Klickitat Drive samples using their original sample vessel. Thus, I retested these two samples using the modified ring shear sample vessel for comparison. The Ledgewood, Discovery Park and Woodway were chosen as the remaining samples because there was no prior knowledge of available shear strength data on these soils.

The sample vessel I used in this study is a two-piece vessel that consists of a lower plate, also known as the lower platen, and an upper platen (Figure 13). The lower platen had been custom modified for WSDOT to have a base that can be vertically adjusted, in contrast to the original sample vessel that was non-adjustable. The purpose for having a vertically adjustable vessel base is to compensate for the change in thickness of the sample resulting from the consolidation phase. This vertical adjustment allows the recessed surface of the consolidated sample to be elevated flush with the surface of the lower platen.

2.4 Hydrometer Tests

Hydrometer tests are used as part of a soil particle size analysis to determine the gradation of the soil fraction that passes a #200 sieve (Das, 2009). Particles belonging to this soil

fraction are the silt- and clay-sized particles. The clay-size fraction (CF) can be determined from the gradation results as a percentage of the silt- and clay-sized soil fraction. CF is useful information for seeing how the percent clay in the sample correlates with the liquid limit and angle of residual shear strength. WSDOT had performed hydrometer tests on the Oso, Klickitat Drive, and the SR-520 and provided the CF for those five samples. I performed hydrometer tests at the State Materials Testing Laboratory on the Ledgewood, Discovery Park, and Woodway samples following the hydrometer test procedure outlined in the American Association of State Highway and Transportation Officials (AASHTO) Standard Method of Test T 88: Particle Size Analysis of Soils (AASHTO, 2008).

3.0 Results

Through the course of this project I prepared a total of 56 X-ray diffractograms consisting of the seven chemical and heat treatments performed on the <2μm fractions of the eight clay samples. Additionally, I conducted ring shear tests on a subset of five clay samples, and performed hydrometer tests on a subset of three silt- and clay-sized sample fractions. I provide detailed data descriptions along with XRD diffractograms in the Appendix, where data are arranged by geographical sample site location from north to south (Figure 1).

The results of the strength assessments show that the Atterberg limit tests produced a broad array of liquid limits ranging from 33 for the Klickitat Drive sample to 83 for the Woodway sample, and a more limited band of plastic limits ranging of 25 for the SR-520 Shaft 18 sample to 35 for the Woodway sample (Table 2). The LL and Pl values yielded plasticity indices that range from 6 for the Klickitat Drive sample to 48 for the Woodway sample. The clay-size fraction of each sample varied greatly from 10% for the Klickitat Drive sample to 90% for the Woodway sample. Ranges for the angles of residual shear strength based on the normal stress loads of 50-700 kPa went from10-12° for the SR-520 Shaft 7 sample to 28-32° for the Klickitat Drive sample.

The XRD analyses show that seven of the eight clay samples have an identical mineralogy consisting of illite, chlorite and smectite. The Ledgewood sample is the exception because it lacks smectite (Figure 10). Non-clay minerals appearing in all of the diffractograms were inferred to be amphibole and plagioclase, based on the closest matching diffraction data in published mineral diffraction tables (Pei-Yuan, 1977). The clay minerals were identified by their

response to specific treatments. The illite diffraction peaks did not respond to solvating the Mg-saturated samples with glycerol, ethylene glycol, and heating to 550 °C (Figure 14). Chlorite was identified by heating the Mg-sample to 550 °C, which increased the height of the 001 diffraction peak and collapsed the 002 peak (Figure 15). Smectite was identified by solvation with ethylene glycol, which caused the mineral to expand and the 001 peak to shift to a lower 2θ angle (Figure 16). These XRD results agree well with earlier mineralogical studies on Puget Sound clays that show a similar clay mineral composition of illite, chlorite and smectite (Mullineax, 1967).

4.0 Discussion

The goals of this study were to 1) determine the mineral composition of glaciolacustrine clays associated with known landslide deposits, 2) see what correlation exists between the mineralogy and the residual shear strength, and 3) contribute data on strength properties of these clays. The XRD analyses revealed a similarity in clay mineralogy among all of the clay samples. This suggests that the glaciolacustrine clay-size fraction (CF) has a relatively uniform composition, with the possible exception of smectite, over a relatively large geographic area. Presumably, this is because these clay minerals were derived from the same glacial advance source area.

The angle of residual shear strength varies among the samples even though the mineralogy remains the same. However, the XRD analyses conducted in this study identify the mineral types that are present in the samples without providing information on relative mineral percentages. This lack of quantitative information makes the extent to which the mineralogy affects the strength of the clays difficult to determine. Hence, other factors such as CF appear to influence the residual shear strength of these samples more strongly than the mineralogy. For example, the general trend in the relationship between CF and the angle of residual shear strength (ϕ_r) is that ϕ_r decreases with increasing CF (Figure 17). Scatter about the trendline indicates that this relationship is not true for every sample, and that variability in this relationship exists between the slide deposit locations. Additionally, scatter about the trendline among the SR-520 samples shows that conditions can vary within short distances along the surface and with depth in a single deposit. This results from using a limited number of single point samples to characterize deposits that are infinitely larger in extent compared to the size of the soil sample. Thus, establishing a description of the deposit that accurately relates the clay mineralogy and the

strength characteristics would require many more samples from different locations and depths from each deposit.

The results of the ring shear test agree well with the expected values calculated from values for ϕ_r from empirical formulas developed by Dr. Timothy Stark of the University of Illinois at Urbana-Champaign based on CF and LL (Figure 18 and Table 2). Exceptions are the ϕ_r values for the Oso sample and the Discovery Park sample, which plot above the black trendlines designated for the >50% clay-size fraction (Figure 18). Dr. Stark developed four formulas that model the expected ϕ_r values for normal stress loads of 50, 100, 400 and 700 kPa. Thus, for consistency in comparing the measured ϕ_r values to the calculated values, the measured ϕ_r value discussed in the methods and in Table 1 for the 25 kPa normal stress load (Step A) are omitted.

The Oso ϕ_r results compare favorably between the test using the adjustable platen in this study and the test WSDOT performed using the non-adjustable platen. However, it is interesting to note that both tests came in higher than the expected value based on a CF of 56% and a LL of 64. In the case of the Oso sample, the departure from the expected value may include the presence of coarse-grained particles in the ring shear sample. In the case of the Discovery Park sample, in the absence of a prior test for comparison, the departure may be because of procedural errors in the ring shear test. As pointed out earlier in this discussion, these results also show the overarching issue of the variability inherent in these landslide deposits. A greater number of samples from each deposit would likely improve the comparison between the measured ϕ_r values and the expected ϕ_r values.

5.0 Conclusion

This study showed that the mineralogy of the glaciolacustrine clays of the Puget Lowland to consist of a homogeneous assemblage of the clay minerals chlorite, illite and smectite based on samples obtained from known landslide deposits. The qualitative nature of the X-ray Diffraction analyses revealed the identity of the constituent minerals, but provided no information on relative mineral quantities in the samples. Thus, the extent to which the mineralogy controls the strength characteristics of the clay deposits is difficult to determine. The strength of the clays, as expressed by the angle of residual shear strength (ϕ_r) ranges from 11° to 32°. Clay liquid limits had a wide range of 33 to 83, plastic ranged more narrowly between from 25 to 35, plasticity indices ranged from 6 to 48, and sample clay-size fractions covered a wide

range from 10% to 90%. This study shows that, in general, the residual shear strength varies inversely to the clay fraction of the samples, though this relationship is more complex in several cases. The ring shear test results agreed well with expected ϕ_r values calculated from formulas based on CF and LL values with the exception of the Oso and Discovery Park samples, which had higher than expected measured ϕ_r values. The variability observed in the strength data illustrates the inherent conditional variability with space and depth within the landslide deposits. A larger number of samples from various points within each deposit, along with quantitative mineralogical analysis, would allow for more accurate conclusions to be drawn about the relationship between the mineralogy of the glaciolacustrine clays and the strength characteristics.

References Cited

AASHTO, 2008, Standard Method of Test T-88-00, Particle Size Analysis of Soils: Washington DC, www.transportation .org, Accessed March 2015.

ASTM, 2010, Standard D4318 – 10e1, Standard Test Methods for Liquid Limit, Plastic Limit, and Plasticity Index of Soils: West Conshohocken, Pennsylvania, ASTM International, DOI: 10.1520/D4318, www.astm.org, Accessed March 2015.

ASTM, 2011, Standard D2487 – 11, Standard Practice of Classification of soils for Engineering Purposes (Unified Soil Classification System): West Conshohocken, Pennsylvania, ASTM International, DOI: 10.1520/D4318, www.astm.org, Accessed March 2015.

ASTM, 2013, Standard D6467 – 13, Standard Test Method for Torsional Ring Shear Test to Determine Drained Residual Shear Strength of Cohesive Soils: West Conshohocken, Pennsylvania, ASTM International, DOI: 10.1520/D6467, www.astm.org, Accessed February 2015.

Bain, J.A., 1971, A plasticity chart as an aid to the identification and assessment of industrial clays: Clay Minerals, The Mineralogical Society of Great Britain, pp. 1 – 17.

Baum, R.L., Chleborad, A.F., and Schuster, R.L., 1998, Landslides Triggered by the Winter 1996-97 Storms in the Puget Lowland, Washington: U.S. Geological Survey Open-File Report 98-239, http://pubs.usgs.gov/of/1998/ofr-98-239/ofr-98-239.html, Accessed March 2015.

Bartoy, K., 2014, Section 106 PA Exemptions Tracking Report, Interstate 5 (I-5) – Klickitat Drive Landslide: http://www.wsdot.wa.gov/NR/rdonlyres/DC75997D-C498-4BE1-8E23-BF7DDD90C315/0/ExemptionsRptMay2014.pdf (May 2014), Accessed March 2015.

Borchardt, G., 1977, Clay mineralogy and slope stability: California Division of Mines and Geology, Special Report 133, pp. 1 – 15.

Das, B.M., 2009, Soil Mechanics Laboratory Manual: Oxford University Press, Inc., New York, NY, 10016, 299 p.

Dragovich, J.B., Stanton, B.W., Lingley, Jr., W.S, Griesel, G.A., and Polenz, M., 2003, Geologic Map of the Mount Higgins 7.5-minute Quadrangle, Skagit and Snohomish Counties, Washington: Washington State Department of Natural Resources, Open File Report 2003-12.

Gordon, R.J., and Cool, S.W., 2013, Ledgewood Landslide Evaluation, Whidbey Island: GeoEngineers, Inc., Bellingham, WA, File No. 0422-097-00, 30 p. Report copy provided by GeoEngineers, Inc., Bellingham, WA, 2014.

Moore, D.M., and Reynolds, Jr., R.C., 1997, X-Ray Diffraction and the Identification and Analysis of Clay Minerals: Oxford University Press, Inc., New York, NY 10016, 378 p.

Mullineaux, D.R., Waldron H.H., and Rubin, M., 1965, Stratigraphy and Chronology of Late Interglacial and Early Vashon Glacial Time in the Seattle Area, Washington: Contributions to Stratigraphy, U.S. Geological Survey Bulletin 1194-0, pp. 1 – 11.

Mullineaux, D.R., 1967, Gross Composition of Pleistocene Clays in Seattle, Washington: U.S. Geological Survey Professional Paper 575-B, pp. B69 – B76.

NYDOT, 2007, Test Method for the Liquid Limit, Plastic Limit, and Plasticity Index: Geotechnical Test Method GTM-7, Revision #1: New York State Department of Transportation Geotechnical Engineering Bureau, pp. 1 – 16.

O'Hagan, M., 2013, Big Landslide on Whidbey Island: Seattle Times, http://blogs.seattletimes.com/today/2013/03/king5-big-landslides-on-whidbey-island/ (March 2013), Accessed March 2015.

Pei-Yuan Chen, 1977, Table of Key Lines in X-ray Powder Diffraction Patterns of Minerals in Clays and Associated Rocks: Indiana Department of Natural Resources, Geological Survey Occasional Paper 21, 67 p.

Perkins, D., 2002, Mineralogy: Prentice-Hall, Inc., Upper Saddle River, New Jersey 07458, 483 p.

Poppe, L.J., Paskevich, V.F. Hathaway, J.C., and Blackwood, D.S., 2001, A Laboratory Manual for X-Ray Powder Diffraction: U.S. Geological Survey Open-File Report 01-041, 88 p.

Reddy, K., 2002, Engineering Properties of Soils Based on Laboratory Testing: Department of Civil and Materials Engineering University of Illinois at Chicago, 178 p.

Robertson, J., 2014, Landslide in Washington State: U.S. Geological Survey Science Features, http://www.usgs.gov/blogs/features/usgs_top_story/landslide-in-washington-state/ (April 2014). Accessed February 2015.

Savage, N.Z., Morissey, M.M., and Baum, R.L., 2000, Geotechnical Properties for Landslide-Prone Seattle Area Glacial Deposits: US Geological Survey Open File Report 00-228, pp. 1 – 5.

Stark, T.D., 2012, Expert Report: Geotechnical Evaluation of Quaternary Pre-Vashon/ Glaciolacustrine (QPGL) Clay, SR-520 Bridge Replacement, Bellevue, Washington: Washington State Department of Transportation, 74 p. Report copy provided by WSDOT, 2015.

Stark, T.D., and Hussain, M., 2013, Drained shear Strength Parameters for Analysis of Landslides: Journal of Geotechnical and Geoenvironmental Engineering, v. 139, p. 853 – 862.

Subbarao, E.C., 1953, A Study of the Fundamental Properties of Puget Sound Glacial Clays [Masters thesis]: Seattle, University of Washington, 74 p.

Troost, K.G., and Booth, D.B., 2008, Geology of Seattle and the Seattle area, Washington: The Geological Society of America, Reviews in Engineering Geology, v. 20, pp.

Tubbs, D.W., 1974, Landslides in Seattle: Washington State Department of Natural Resources, Division of Geology and Earth Resources, Circular No. 52.

West, T., 1995, Geology Applied to Engineering: Prentice Hall, Englewood Cliffs, NJ 07632, 542 p.

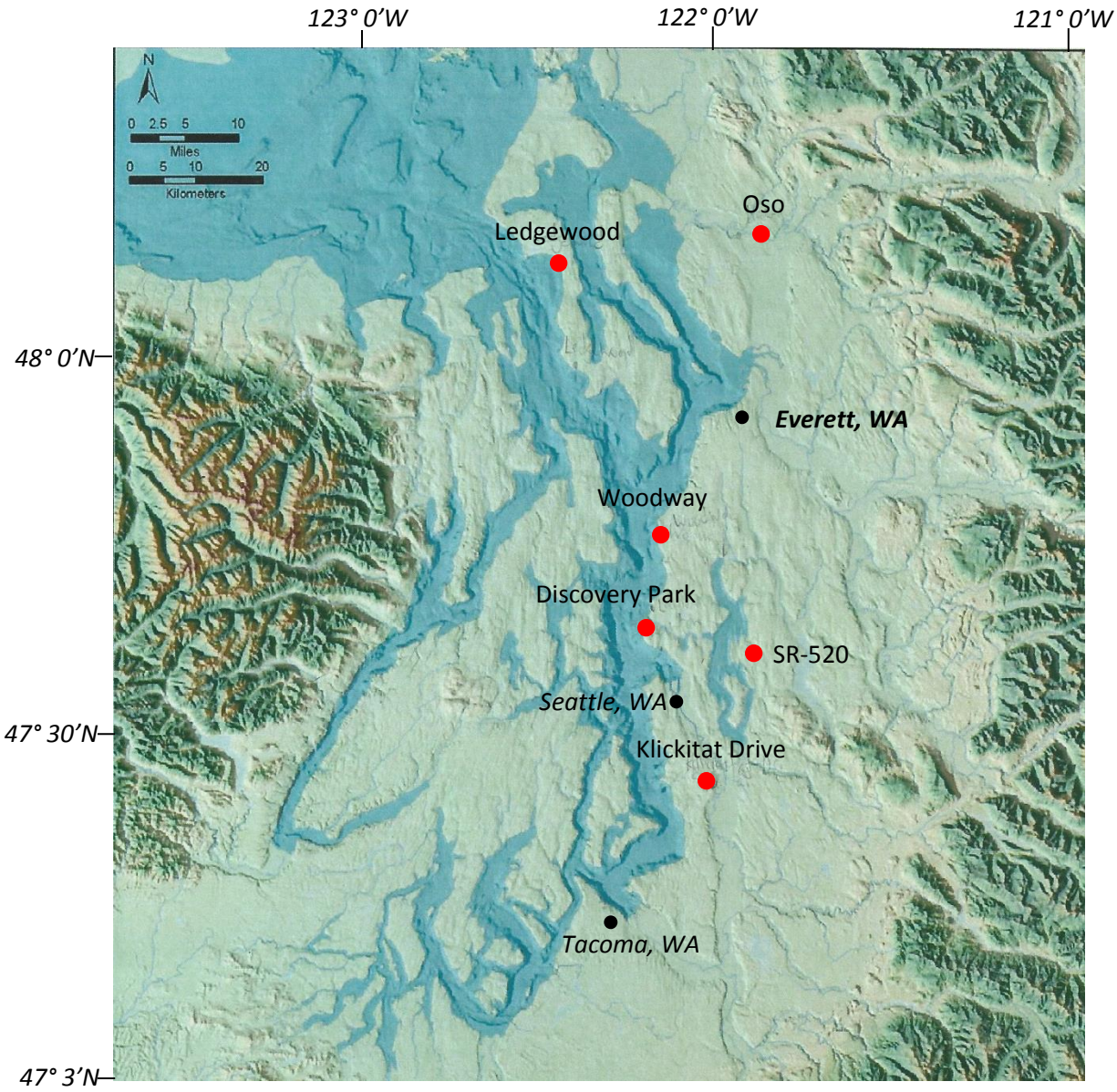

Figure 1. Overview of the Puget Lowland showing the locations of the sampled landslide deposits (red markers), along with major populations centers for geographical reference. The imprint of continental glaciation on the landscape can be seen through the network of scoured troughs that Puget Sound now occupies. The map coloration indicates topography; blue showing Puget Sound and pale green the lowlands, with green indicating uplands and tan showing the highest elevations (figure adapted from map image courtesy of Kathy Troost, 2015).

Figure 2. Oblique view of the Oso landslide looking east (Robertson, 2014). Runout from the slide can be seen crossing the North Fork of the Stillaguamish River and continuing westward out of view of the photograph. WSDOT provided the clay sample from the glaciolacustrine deposit near the base of the slope. The exact location of the sampling point is unknown to the author.

Figure 3. Oblique aerial view of the Ledgewood slide looking southward. (Seattle Times, 2013).

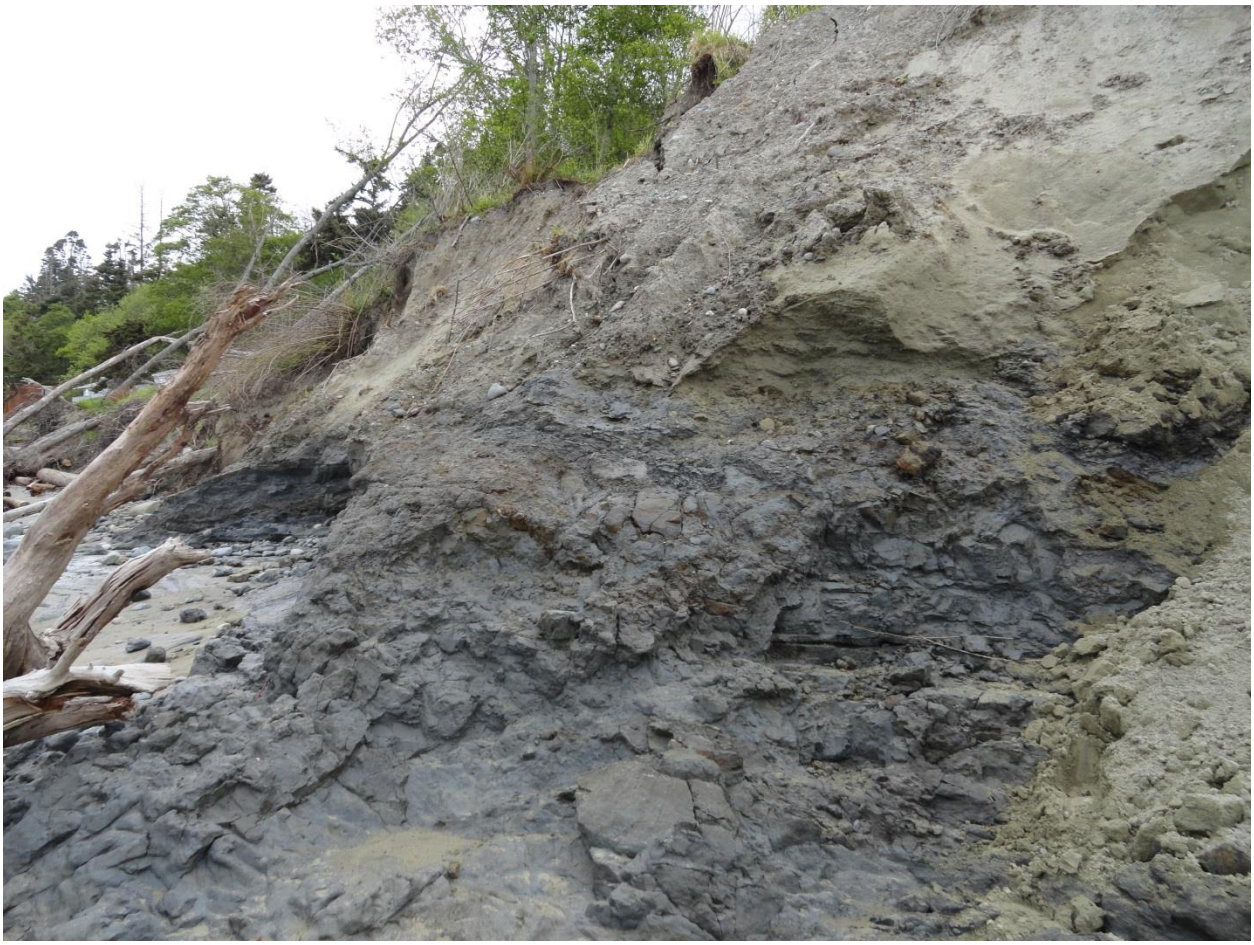

Figure 4. Clay exposed at the sampling location in the toe of the Ledgewood slide. View looks to the northeast (Photo by author, April 2014).

Figure 5. Oblique view of the 1997 Woodway slide looking east in the town of Woodway, WA (Baum et al., 1998). Vegetation has now recolonized the slide surface in the 17 years since this photo was taken. The sampling site is located at approximately three-quarters of the way bluff face along the north edge of the failure surface.

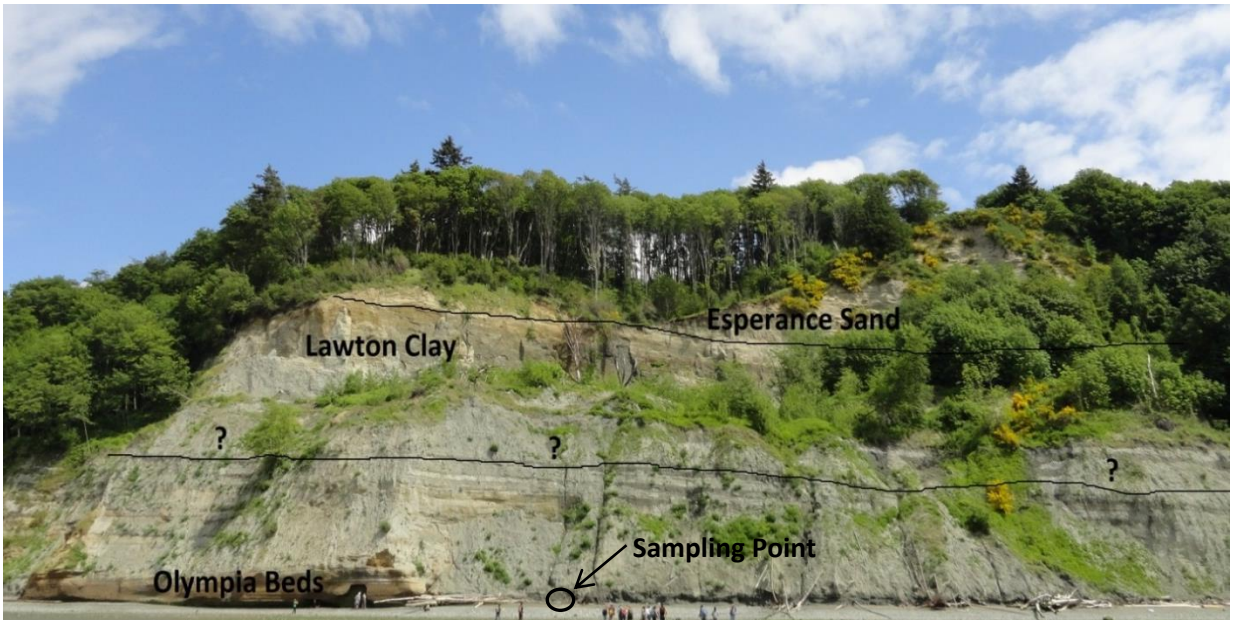

Figure 6. The Vashon glacial sediment deposit sequence exposed above the shore of Puget Sound at Discovery Park in Seattle, WA. In the Seattle area the glaciolacustrine clay deposit is known as the Lawton Clay. Intact blocks of Lawton Clay are accessible from the beach as clay material sluffs down to the base of the bluff. The sampling location was selected for safety reasons and ease of access to the material. The height of the bluff from the base to the small gap in the trees at the highest point is approximately 80 meters. The Lawton clay overlies bedded pre-Vashon sediments deposited during the Olympia nonglacial interval, and is overlain by the Esperance Sand. The cap of glacial till is not present at this exposure. The lower line marks a gradational contact between the Lawton Clay and the Olympia beds (Mullineaux et al., 1965). (Photo by author, taken May 2014).

Figure 7. Photo collage of the 2011 SR-520 slope failure in Bellevue, WA (Stark, 2013). a) East-looking view of the access road excavation. The old off-ramp to Bellevue Way sits on top of the plastic-covered graded slope, and the exposed clay can be seen sticking out at the slope base. b) Tension cracks developing just below the surface at the top of the old off-ramp. c) View looking down on the old Bellevue Way off-ramp surface showing pavement damage produced by slope movement. d) Eastward view of slope from the old Bellevue Way off-ramp surface showing the slope movement retrogressing upslope.

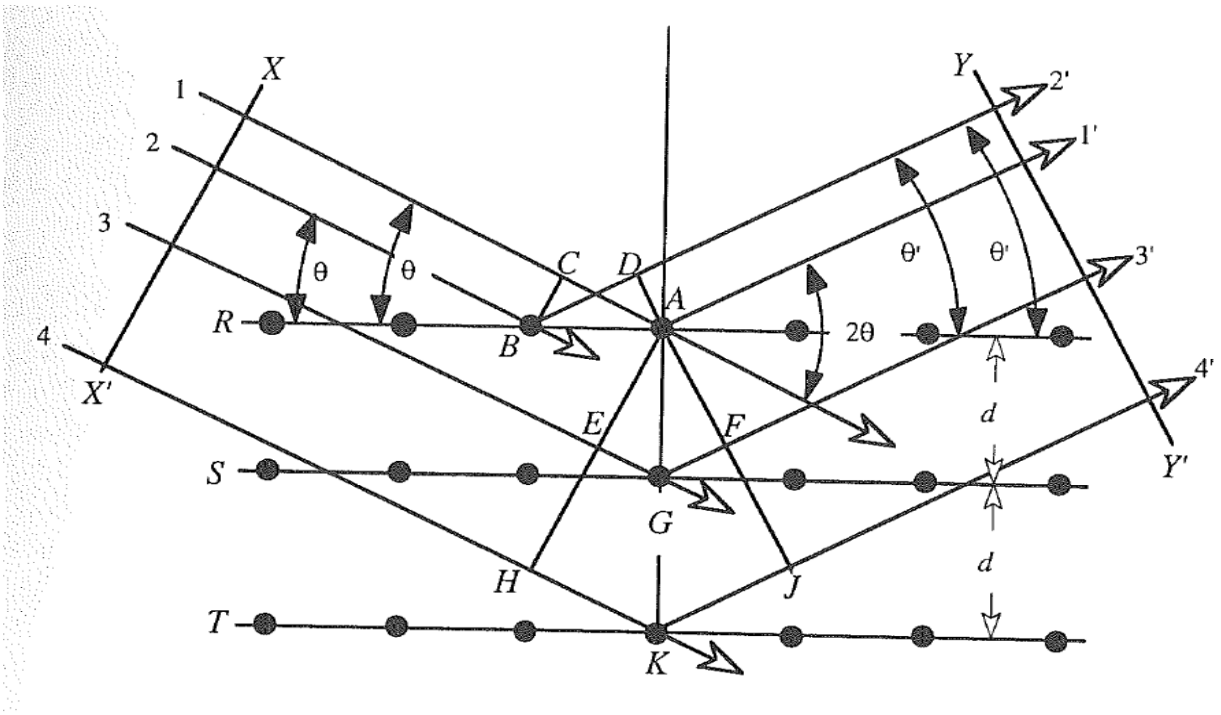

Figure 8. Diagram illustrating X-ray diffraction from the atomic planes of a clay mineral. Each X-ray incident at angle θ traveling along the wave front X-X' penetrates the mineral surface and is diffracted from the atoms in atomic planes R, S and T separated by distance, d (Å). Constructive interference produces diffracted waves of increased energy when scattered waves leaving the sample are in phase (reproduced from Moore and Reynolds, 1997).

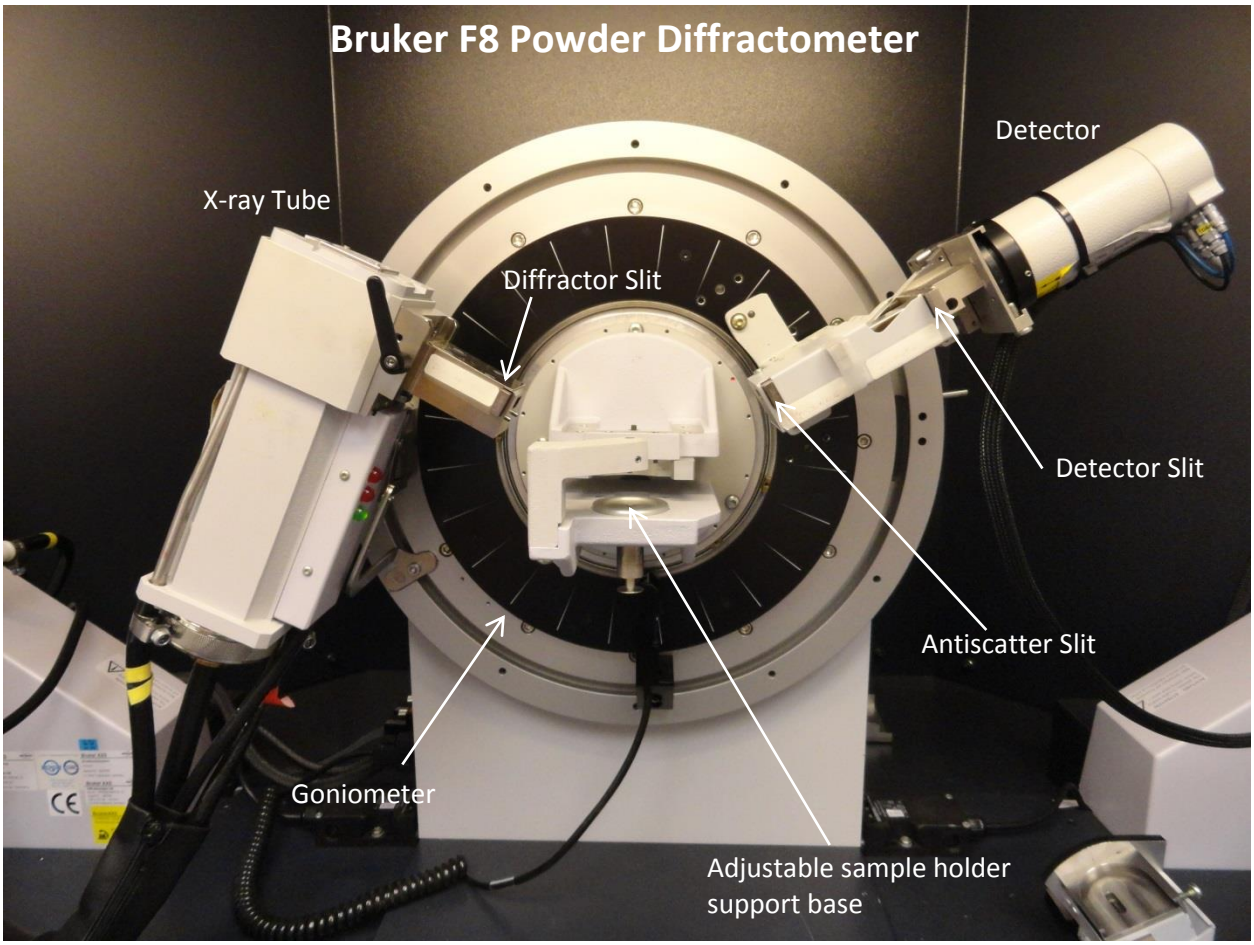

Figure 9. The Bruker F8 Powder X-ray Diffractometer used in this study at the Materials Science and Engineering User Facility on the UW main campus. The device mounted at an angle on the left side of the apparatus is the X-ray tube. The tube focuses an X-ray beam onto the clay sample mounted on a petrographic slide held in a fitted plastic slide holder. The slide holder is held in place on the circular, vertically adjustable metallic support base visible in the center. The surface of the clay sample on the glass slide is held exactly in the X-ray diffraction plane when the support base is adjusted fully upward so that the holder is butted against the bottoms of three guide pins. As the incident X-ray beam exits the tube it passes through the diffractor slit and strikes the clay surface where it is diffracted. The device mounted at an angle on the right side of the diffractometer is the detector, which receives the diffracted X-rays after they pass through the antiscatter slit, the nickel filter, and finally the detector slit. The detector records the diffraction intensity and transfers this information to the computer analysis software (photo by author, 2014).

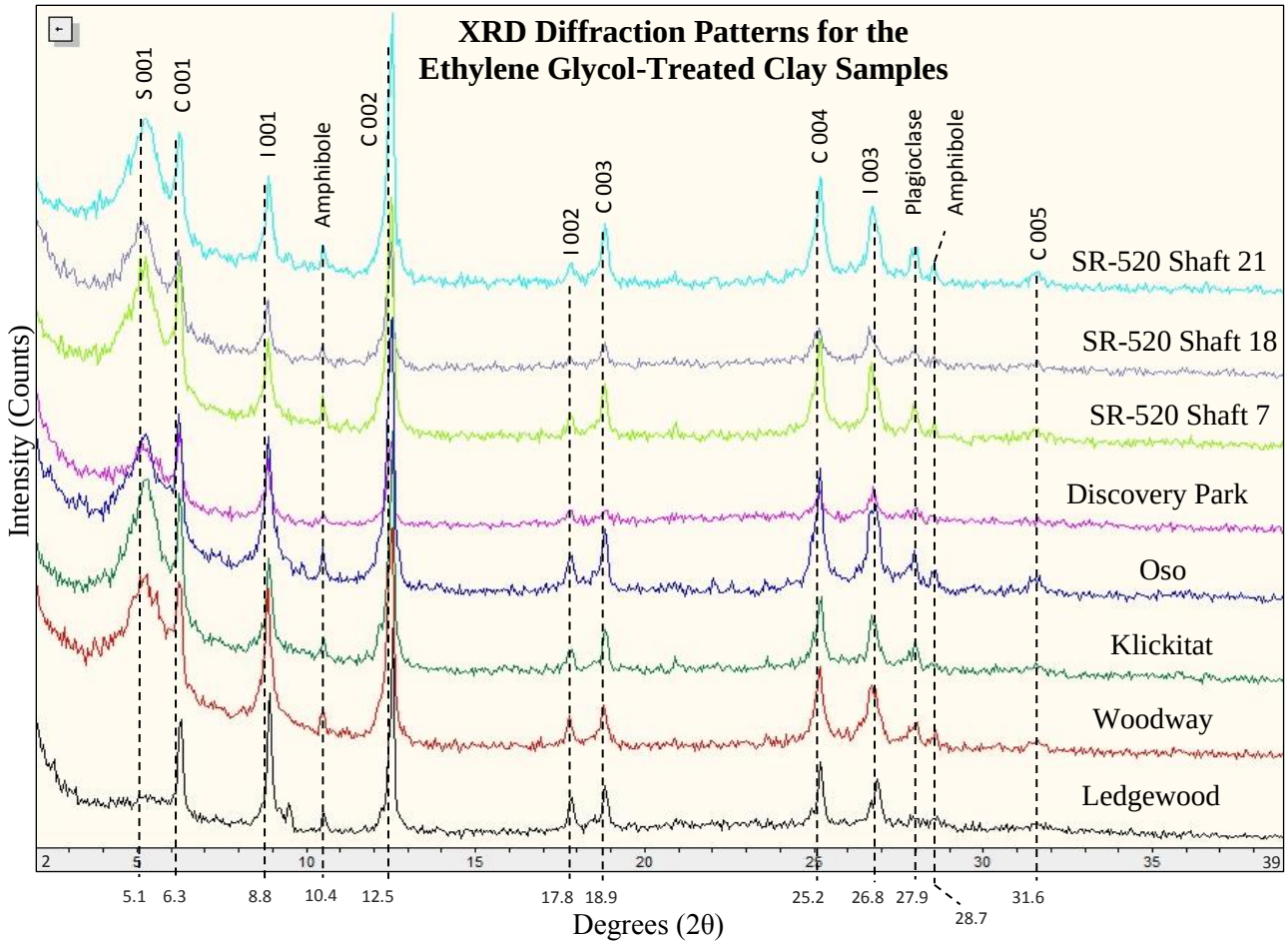

Figure 10. XRD diffractograms of the ethylene glycol-treated clay samples of the clay suite. The glycol-treated diffractograms were used in this illustration so that the smectite peak at approximately 5.1 degrees 2θ would be visible. Note the great similarity of the diffractogram patterns for all the samples in terms of 2θ peak locations. This similarity shows that the composition of the clays is essentially identical, with the exception of a lack of smectite in the Ledgewood sample, indicated by missing S001 peak. C001, C002, C003, C004, and C005 are the first, second, third, fourth and fifth order chlorite diffractions; I001, I002, I003 are the first, second and third order illite diffractions; S001 is the first order smectite reflection.

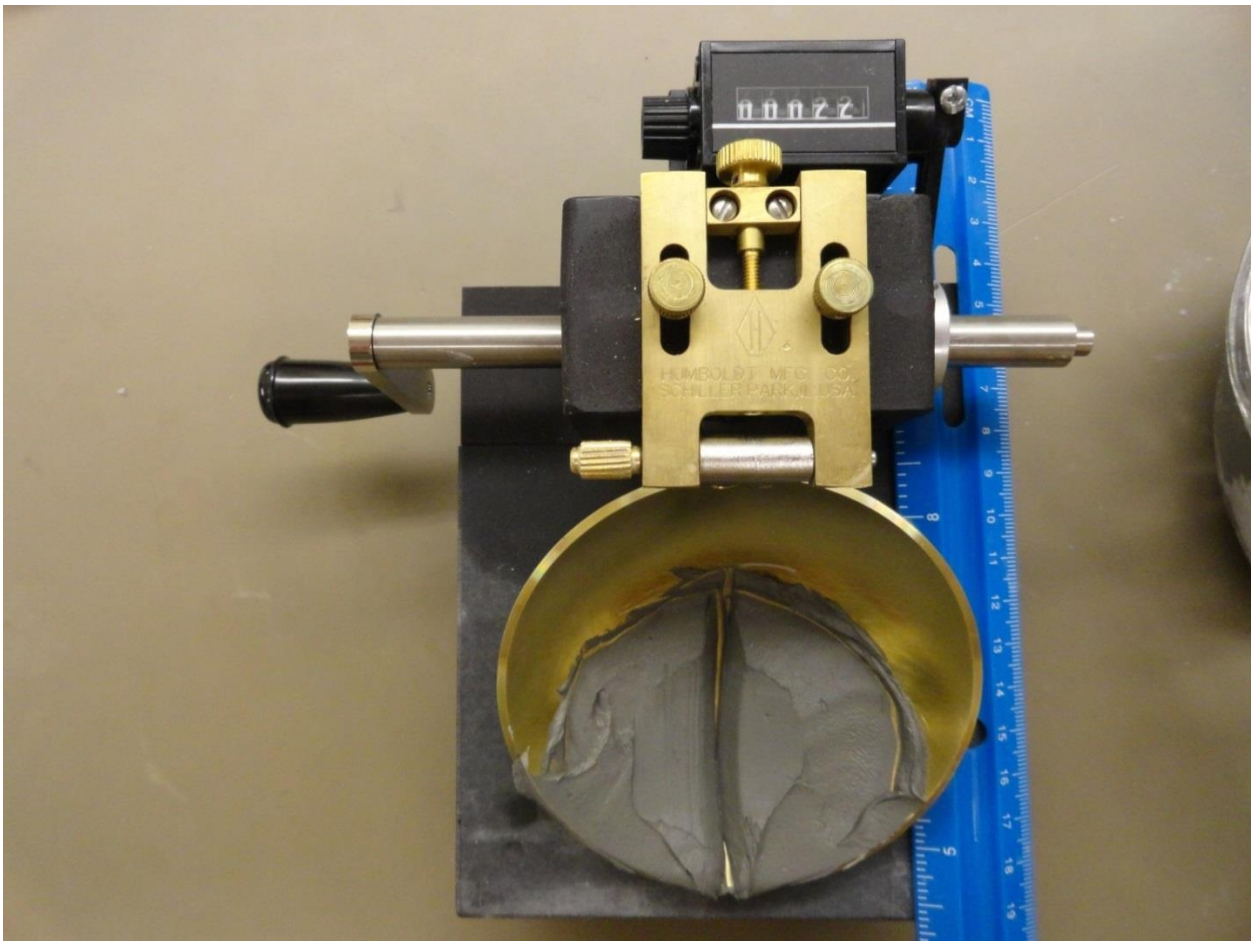

Figure 11. A standard LL apparatus showing the results of a LL test. The two halves of the clay cake are shown having closed together across a groove of standard dimensions cut through the cake. The number 22 on the counter shows the number of drops from a height of 10 mm it took to draw the two halves together over a distance of approximately 13 mm (ASTM 4318-10) (photo by author, 2014).

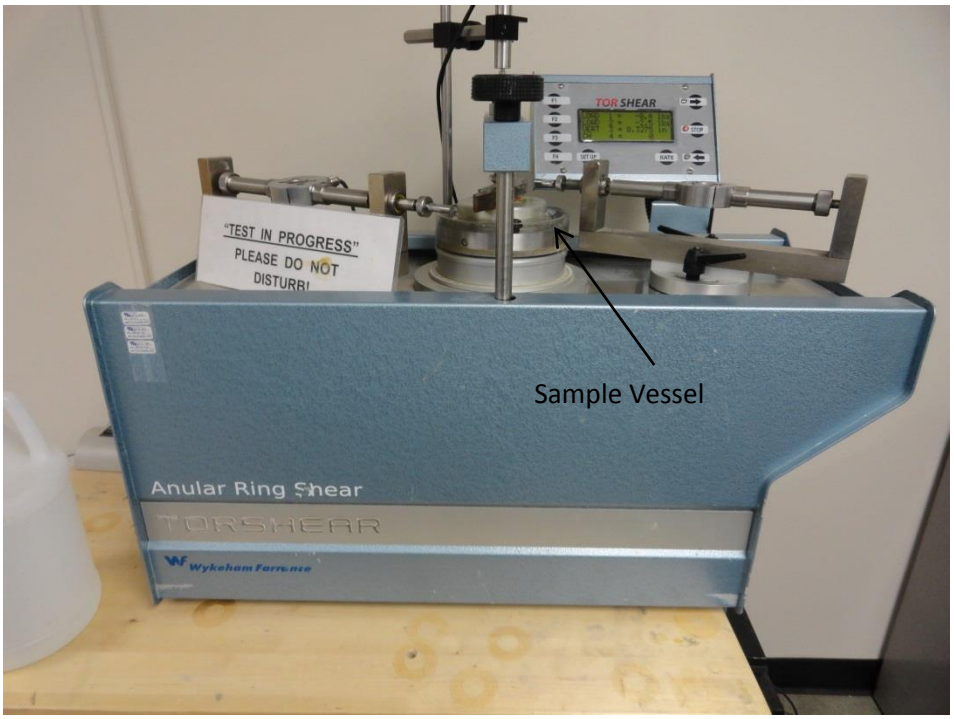

a)

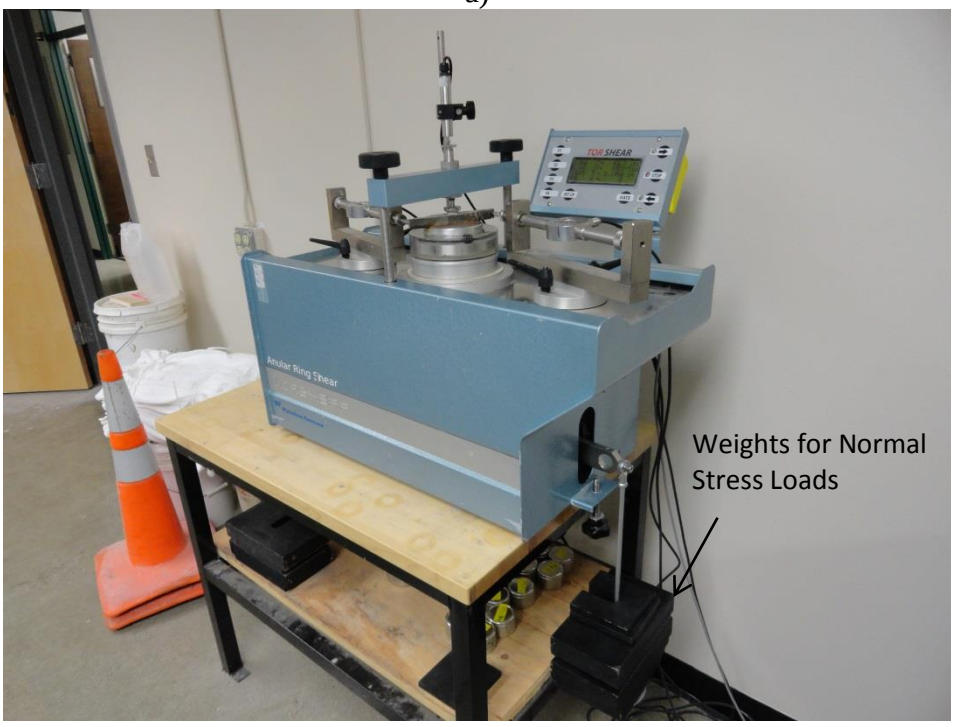

b)

Figure 12. Photographs of the ring shear test apparatus. a) The two mechanical arms on the left and right of the machine hold the upper platen of the sample vessel in place while the base supporting the lower platen slowly rotates, shearing the clay at 0.024 inches per minute. b) View of the machine shearing the clay under the 700 KPa (29 kg applied weight) step D normal stress load.

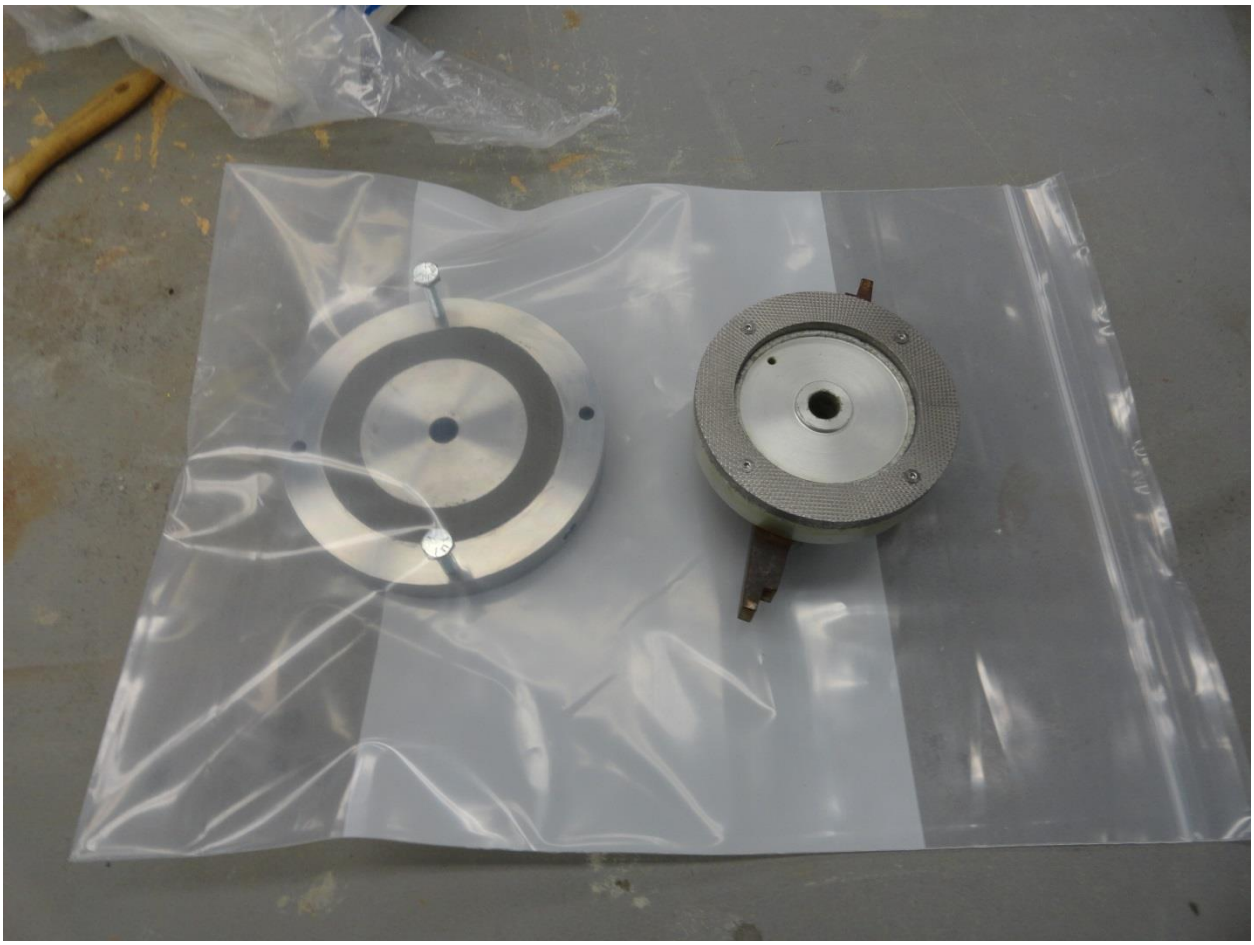

Figure 13. Photograph of the upper and lower platens of the ring shear sample vessel. The lower platen is the piece shown sealed in a plastic bag to prevent moisture loss from the clay sample loaded in the ring-shaped recess.

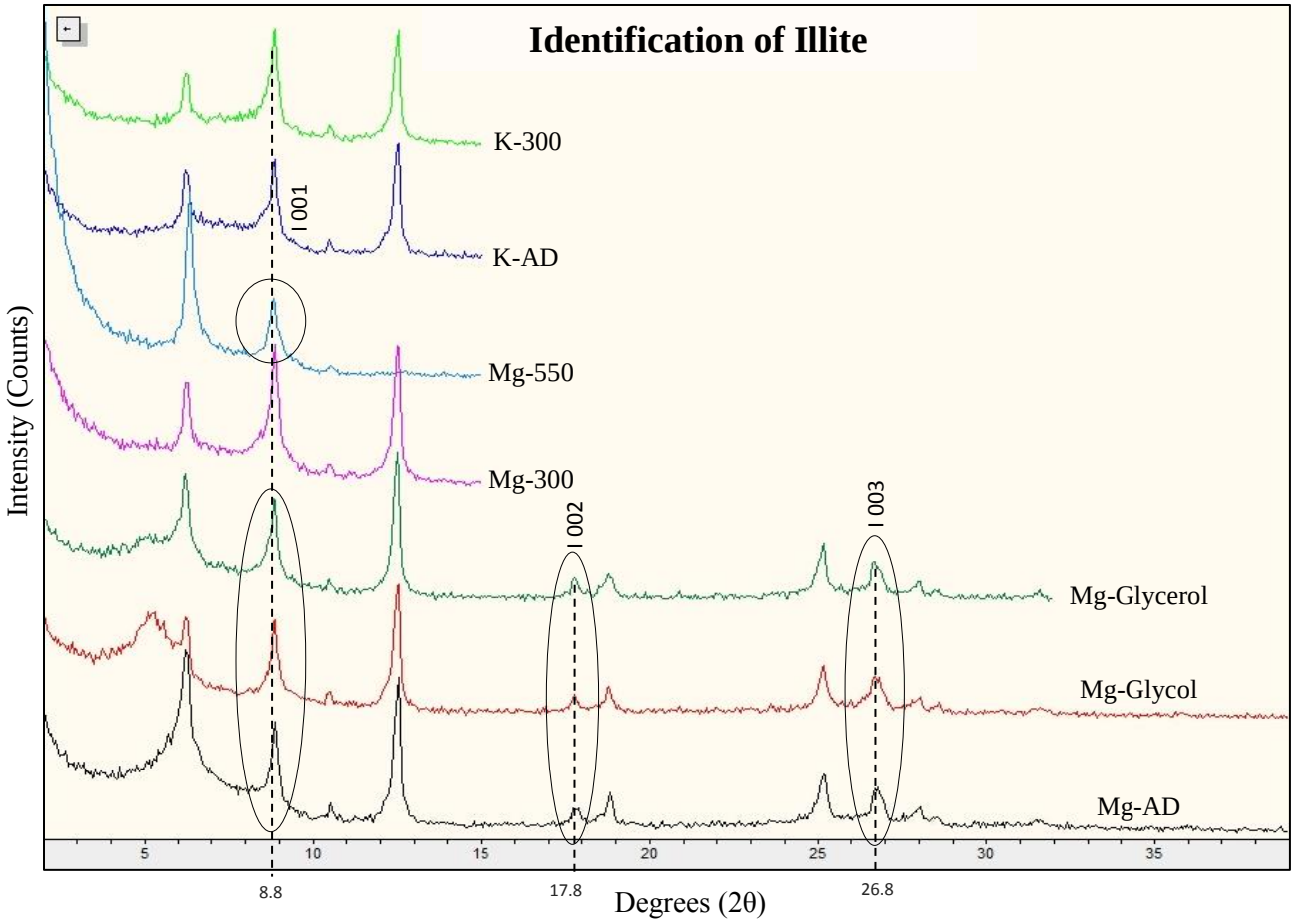

Figure 14. Illustration using the Woodway sample of how the response to treatments aided in identifying illite in the clay samples. The Woodway sample was chosen to represent the sample suite here and in figures 15 and 16 that follow because this sample responded to the treatments in such a way that the subtleties among the sample treatments showed up well. The main diagnostic feature for illite is the lack of response of the illite diffraction peaks to solvation with ethylene glycol, glycerol, or heating to 550 °C. This response is characteristic of illite (Moore and Reynolds, 1997).

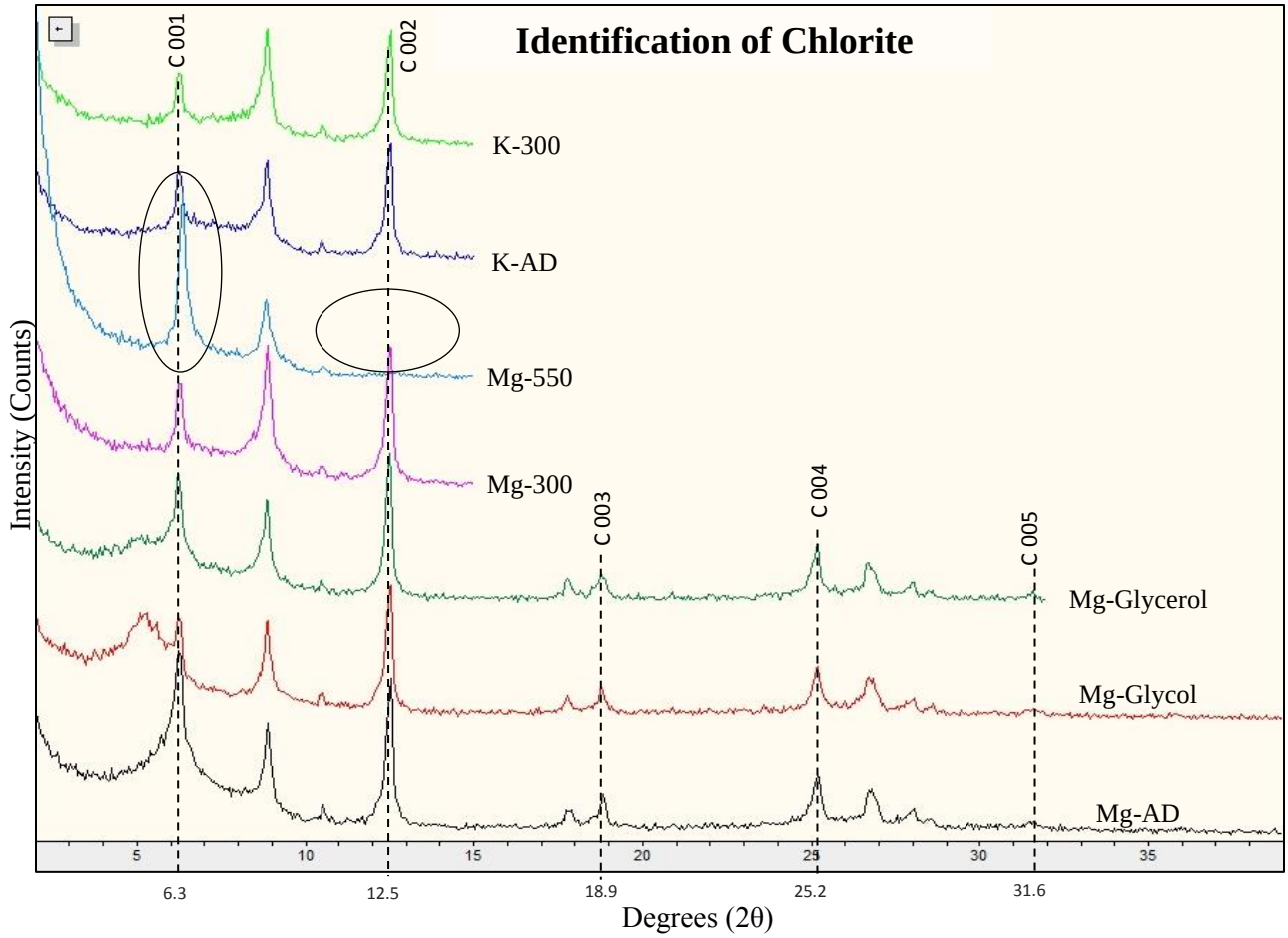

Figure 15. Illustration using the Woodway sample of how the response to treatments aided in identifying chlorite in the clay samples. The Woodway sample was chosen to represent the sample suite here and in figure 14 above and figure 16 below because this sample responded to the treatments in such a way that the subtleties among the sample treatments showed up well. The main diagnostic feature for chlorite was the increase in height of the 001 peak and the collapse of the 002 peak in the Mg-550 diffractogram resulting from heating the Mg-saturated sample to 550 °.

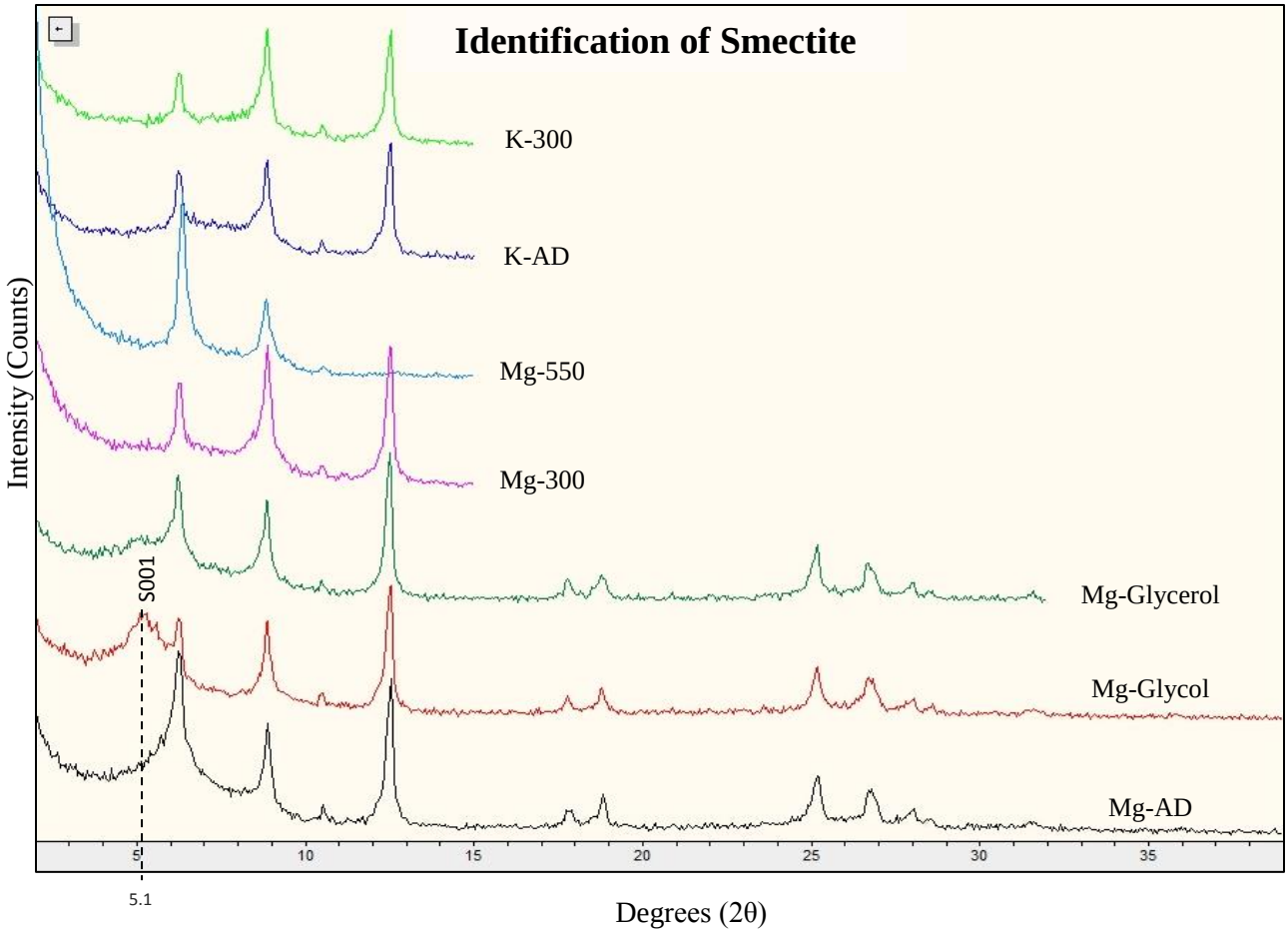

Figure 16. Illustration using the Woodway sample of how the response to treatments aided in identifying smectite in the clay samples. The Woodway sample was chosen to represent the sample suite here and in figures 14 and 15 above because this sample responded to the treatments in such a way that the subtleties among the sample treatments showed up well. The diagnosis for smectite came from the broad smectite 001 peak in the Mg-Glycol diffractogram resulting from swelling of the smectite mineral structure in response to solvation of the Mg-saturated sample with ethylene glycol.

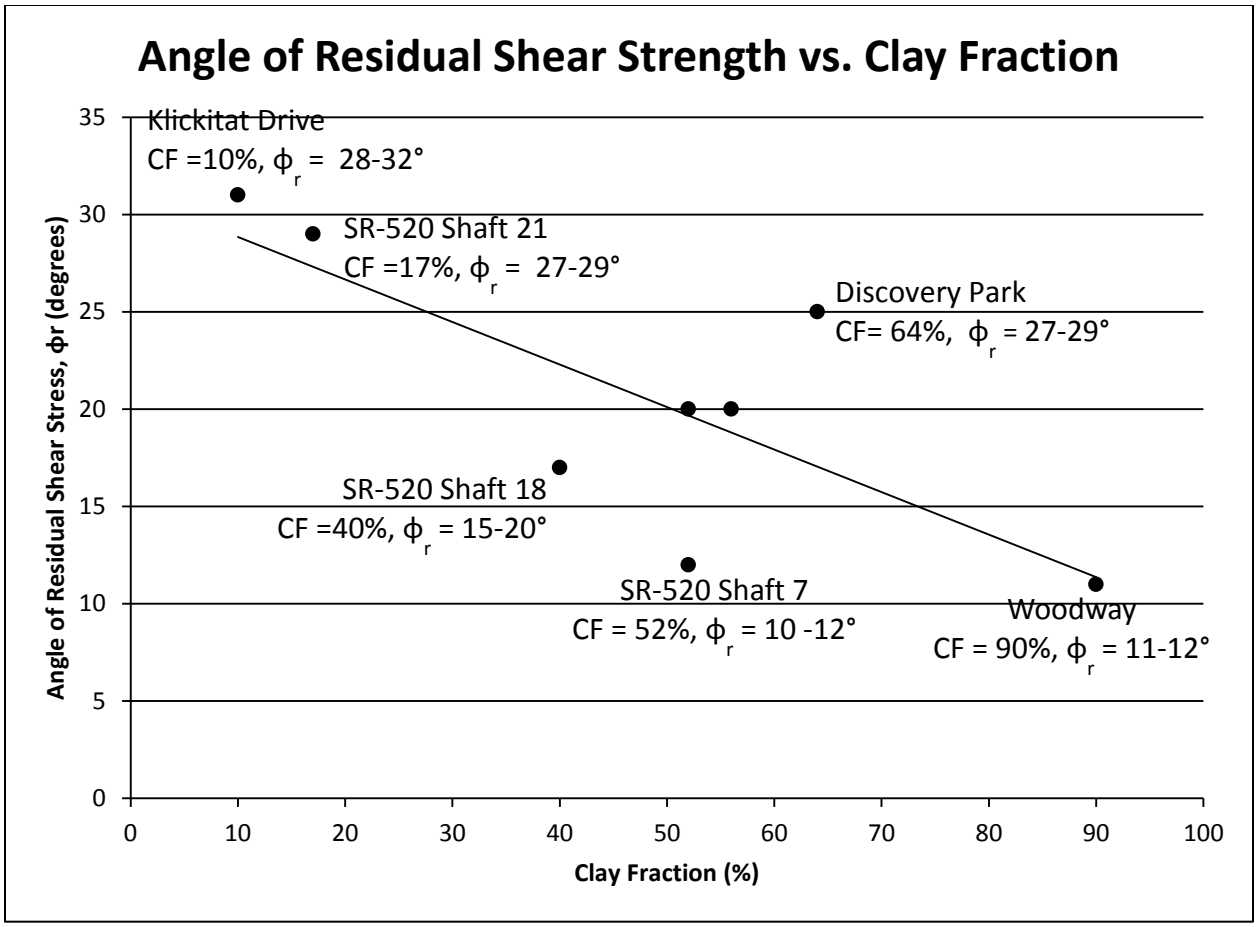

Figure 17. Graph showing the general inverse relationship between clay fraction (CF) and angle of residual shear strength (ϕ_r). Scatter between samples such as Discovery Park and SR-520 Shaft 7 shows that this trend is not constant. The scatter among the SR-520 samples shows how conditions can vary within a single deposit.

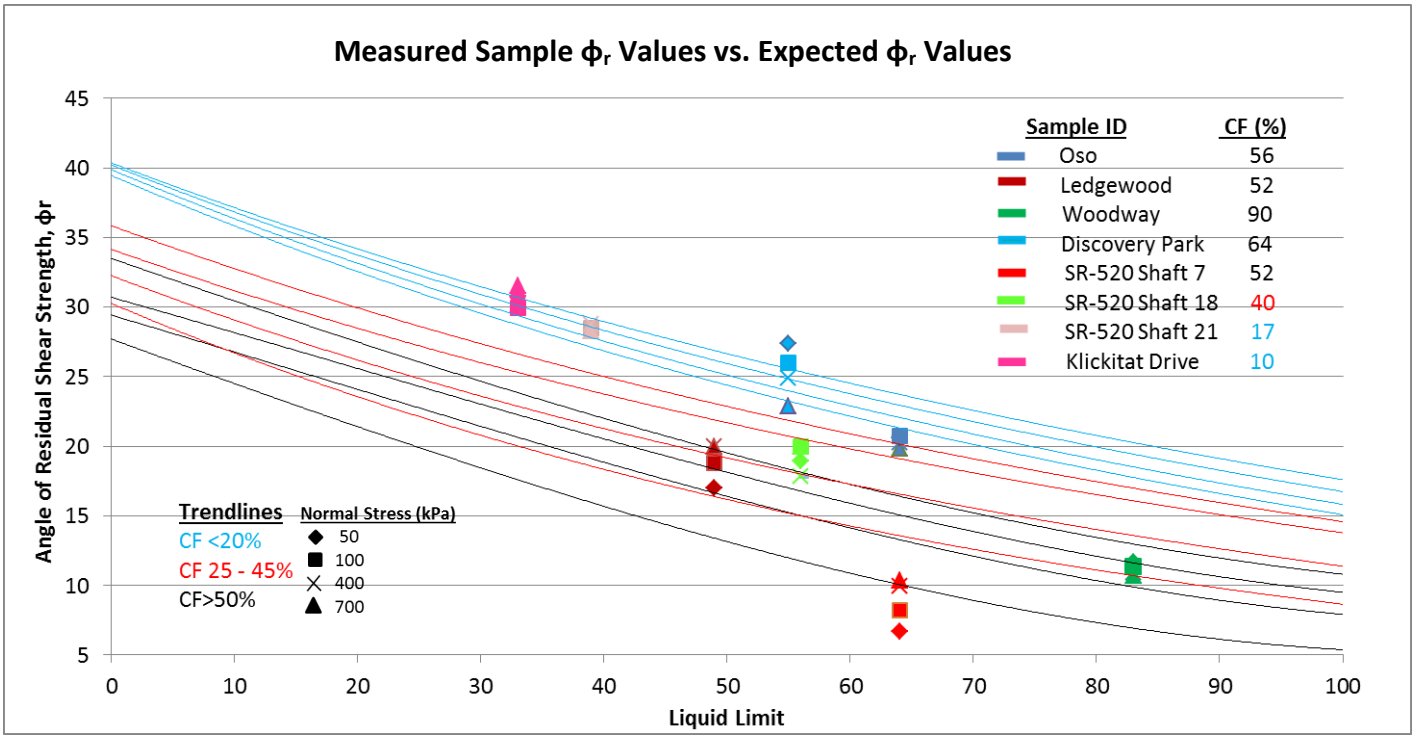

Figure 18. Comparison of the measured angle of residual shear strength values to the expected shear strength angles based on the formulas developed by Dr. Timothy Stark (Stark, 2013). The trendlines are colored according to clay-size fraction (CF) ranges, and the shear stress angles from each of the normal stress loads for each sample are plotted against the trendline curves. In the sample legend, the clay-size fraction values are colored according to their respective CF values for easier plot interpretation.

Table 1. Normal stress loads at steps A, B, C, D and E for both the consolidation phase and the shearing phase of the ring shear test. The normal stress values given here help facilitate comparing residual shear stress angles (ϕ_r) derived from shear tests to expected values of ϕ_r from published stress curves (Figure 15).

Consolidation and Shearing Steps	Normal Stress (kPa)	Applied Weight (kg)
A	25	1.11
B	50	2.15
C	100	4.21
D	400	16.61
E	700	29.00

Table 2. Summary table of the strength attributes of the clay samples analyzed in this study. The samples are listed from top to bottom in the table according to their geographical location from north to south (Figure 1). The values for ϕ_r are given as the range of angles obtained from the ring shear test points at the 50 – 700 kPa normal stress load range of the shear test. The low normal stress value of 25 kPa for point A shown in Table 5 above omitted in this table for purposes of consistency in comparing the results to the four-point normal stresses prescribed in Dr. Timothy Stark's formulas as shown in Figure 18.

Clay Sample Strength Characteristics							
	Atterberg Limits			**Hydrometer Test**	**Residual Shear Test, ϕ_r (°)**		
Sample ID	**LL**	**PL**	**PI**	**CF (%)**	**Measured Values[a]**	**Measured Values[b]**	**Expected Values [c]**
Oso	64	31	33	56	20-21	18-20	10-17
Ledgewood	49	28	21	52	14-20	-	14-20
Woodway	83	35	48	90	11-12	-	7-13
Discovery Park	55	28	27	64	23-27	-	12-18
SR-520-7	64	32	32	52	-	10-12	10-16
SR-520-18	56	25	31	40	-	15-20	16-23
SR-520-21	39	26	13	17	-	27-29	27-30
Klickitat Drive	33	27	6	10	28-32	27-28	29-31

[a] Angle of residual shear strength values measured in this study using the adjustable platen.
[b]Angle of residual shear strength values WSDOT measured using the non-adjustable platen.
[c]Expected values from formulas derived by Dr. Timothy Stark based on clay-size fraction and liquid limit.

Appendix – Data Descriptions

A.1 Oso Landslide

The results of the XRD scans for the Oso sample reflect the presence of chlorite, illite and smectite (Figure 16). The peaks labeled 001, 002, 003, 004 and 005 that respectively occur at approximately 6.3, 12.5, 18.9, 25.2 and 31.6 degrees 2θ designate chlorite; illite is indicated by peaks 001, 002 and 003 occurring at approximately 8.8, 17.8, and 26.8 degrees 2θ; smectite shows up at 001 occurring at approximately 5.1 degrees 2θ. Solvating the sample with ethylene glycol brought out the presence of smectite as seen by the smectite 001 peak in the Mg-glycol pattern. As the Mg-550 pattern shows, heating the sample to 550 °C increased the height of the chlorite 001 peak, and caused the chlorite 002 peak to collapse. Illite was unaffected by treatment with glycerol, ethylene glycol, or heating to 300 °C and 550 °C in neither the Mg- or K-saturated samples.

The results of the residual shear strength tests for the Oso sample yielded a ϕ_r of approximately 20° for the test WSDOT had previously conducted using the non-adjustable sample vessel, and approximately 20° for the test I conducted in this study using the adjustable vessel (Table 2). The Atterberg limit tests yielded a LL of 64, a PL of 31 and a PI of 33, and the hydrometer produced a clay fraction of 56%.

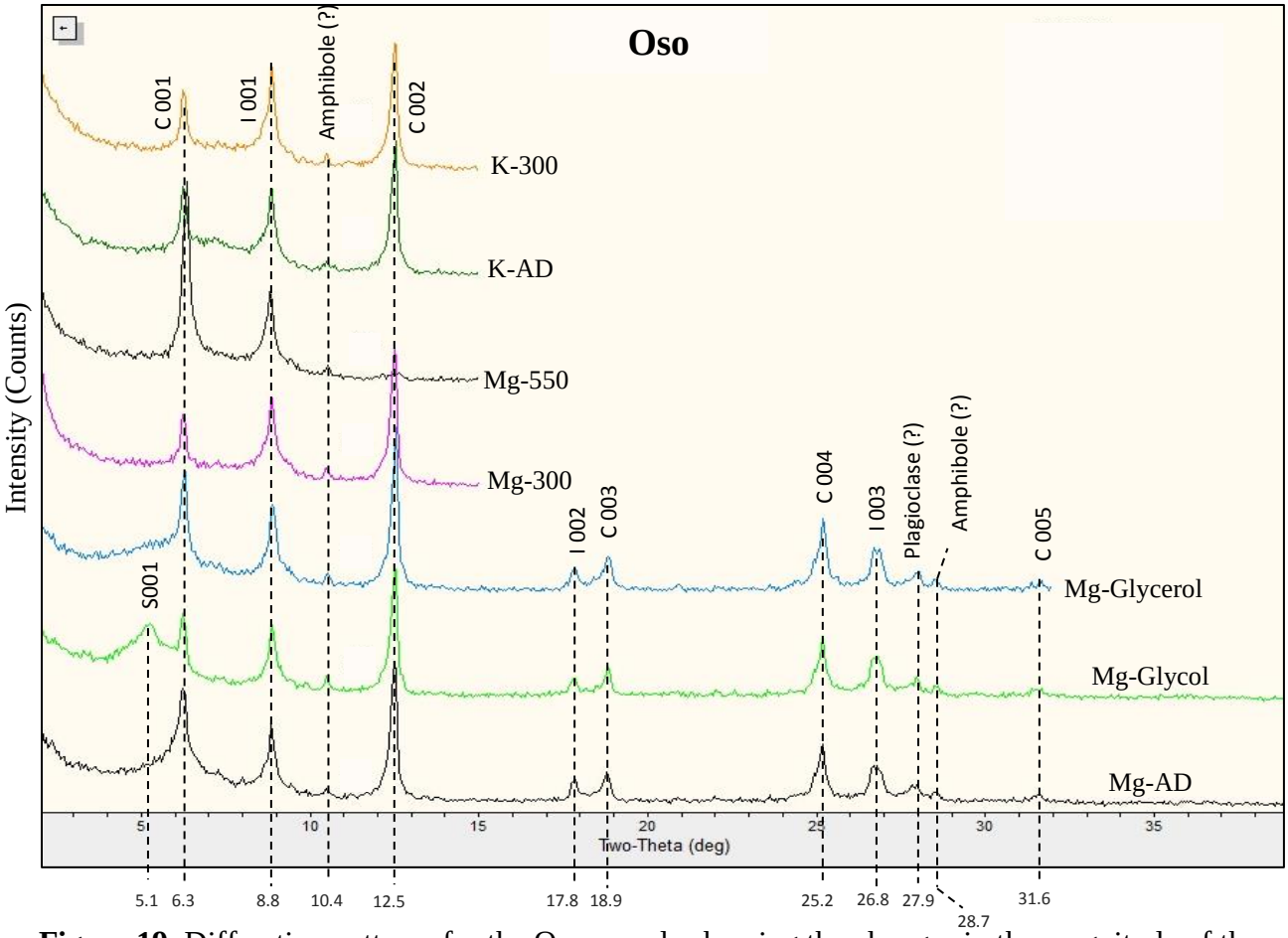

Figure 19. Diffraction patterns for the Oso sample showing the changes in the magnitude of the reflectance peaks in response to the chemical and heat treatments. The patterns for each treatment are labeled as follows: Mg = magnesium chloride-saturated; K = potassium chloride-saturated; AD = air-dried; Glycol = ethylene glycol-solvated; Glycerol = glycerol-solvated; 300 = oven-heated to 300 °C; 550 = oven-heated to 550 °C. I was able to save time through the course of this study by running the Mg-Glycerol scan from 2 to 32 degrees 2θ, and the Mg-300, Mg-550, K-AD, and K-300 patterns from 2 to 15 degrees 2θ. These shorter 2θ ranges were sufficient to capture the effects of these treatments for analytical purposes.

A.2 Ledgewood Slide

The results of the XRD scans for the Ledgewood sample reflect the presence of chlorite, illite (Figure 17). The peaks labeled 001, 002, 003, 004 and 005 that respectively occur at approximately 6.3, 12.5, 18.9, 25.2 and 31.6 degrees 2θ designate chlorite; illite is indicated by peaks 001, 002 and 003 occurring at approximately 8.8, 17.8, and 26.8 degrees 2θ indicate illite. The Ledgewood sample was the only one of the eight samples in which smectite was not present, which would have been observed as a broad peak at approximately 5.1 degrees 2θ in the Mg-glycol diffractogram. As the Mg-550 pattern shows, heating the sample to 550 °C increased the height of the chlorite 001 peak, and caused the chlorite peaks 002, 003 and 004 peaks to collapse. Illite was unaffected by treatment with glycerol, ethylene glycol, or heating to 300 °C and 550 °C in neither the Mg- or K-saturated samples.

The results of the residual shear strength test for the Ledgewood sample yielded a residual stress failure angle (ϕ_r) of approximately 25° (Table 2). The Atterberg limit tests yielded a LL of 49, a PL of 28 and a PI of 21, and the hydrometer test produced a clay fraction of 52%.

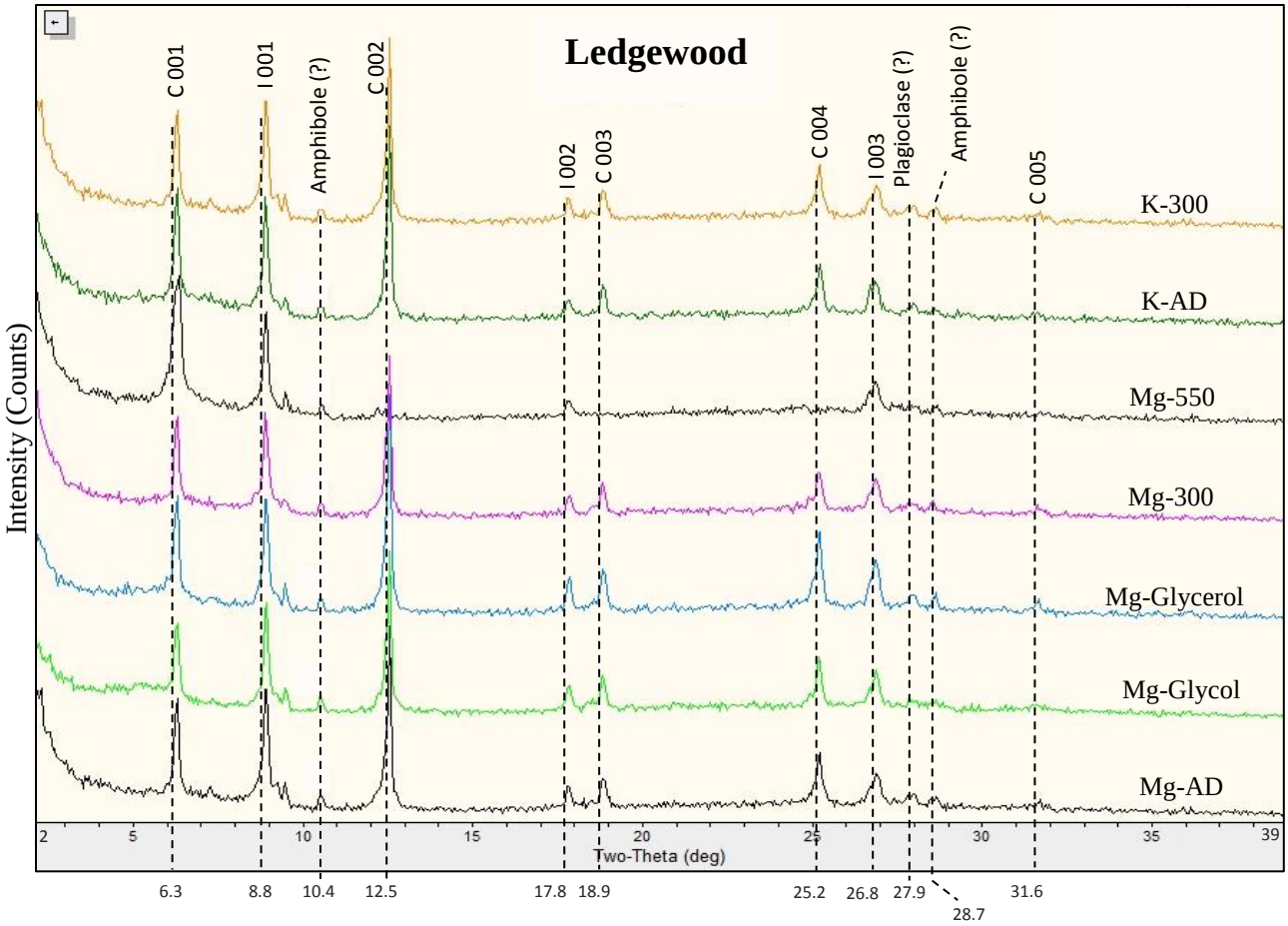

Figure 20. Diffraction patterns for the Ledgewood sample showing the changes in the magnitude of the reflectance peaks in response to the chemical and heat treatments. The XRD scans for the Ledgewood sample were all ran from 2 to 39 degrees 2θ because the Ledgewood sample was used to for training on the diffractometer, and in the process, for establishing the proper diffractometer settings. The treatments are notated in the legend as follows: Mg = magnesium chloride-saturated; K = potassium chloride-saturated; AD = air-dried; Glycol = ethylene glycol-solvated; Glycerol = glycerol-solvated; 300 = oven-heated to 300 °C; 550 = oven-heated to 550 °C.

A.3 Woodway Slide

The results of the XRD scans for the Woodway sample reflect the presence of chlorite, illite and smectite (Figure 18). The peaks labeled 001, 002, 003, 004 and 005 that respectively occur at approximately 6.3, 12.5, 18.9, 25.2 and 31.6 degrees 2θ designate chlorite; illite is indicated by peaks 001, 002 and 003 occurring at approximately 8.8, 17.8, and 26.8 degrees 2θ; smectite shows up at 001 occurring at approximately 5.1 degrees 2θ. Solvating the sample with ethylene glycol brought out the presence of smectite as seen by the smectite 001 peak in diffractogram 2. As diffractogram 5 shows, heating the sample to 550 °C increased the height of the chlorite 001 peak, and caused the chlorite 002 peak to collapse. Illite was unaffected by treatment with glycerol, ethylene glycol, or heating to 300 °C and 550 °C in neither the Mg- or K-saturated samples.

The results of the residual shear strength test for the Woodway sample yielded a ϕ_r of approximately 11° (Table 2). The Atterberg limit tests yielded a LL of 83, a PL of 35 and a PI of 48, and the hydrometer test produced a clay fraction of 90%.

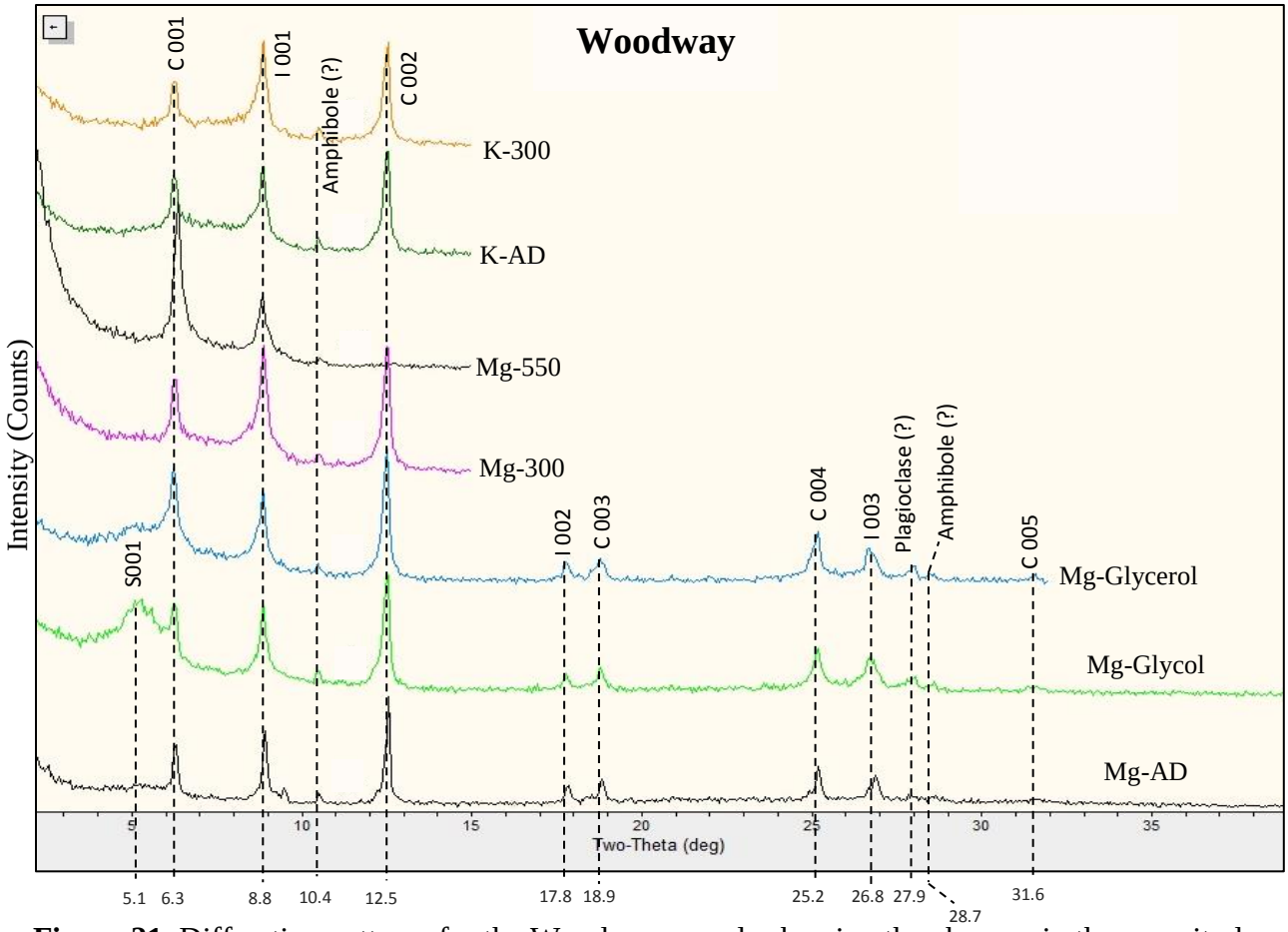

Figure 21. Diffraction patterns for the Woodway sample showing the changes in the magnitude of the reflectance peaks in response to the chemical and heat treatments. The patterns for each treatment are labeled as follows: Mg = magnesium chloride-saturated; K = potassium chloride-saturated; AD = air-dried; Glycol = ethylene glycol-solvated; Glycerol = glycerol-solvated; 300 = oven-heated to 300 °C; 550 = oven-heated to 550 °C. I was able to save time through the course of this study by running the Mg-Glycerol scan from 2 to 32 degrees 2θ, and the Mg-300, Mg-550, K-AD, and K-300 patterns from 2 to 15 degrees 2θ. These shorter 2θ ranges were sufficient to capture the effects of these treatments for analytical purposes.

A.4 Discovery Park

The results of the XRD scans for the Discovery Park sample reflect the presence of chlorite, illite and smectite (Figure 19). The peaks labeled 001, 002, 003, and 004 that respectively occur at approximately 6.3, 12.5, 18.9, and 25.2 degrees 2θ designate chlorite; illite is indicated by peaks 001, 002 and 003 occurring at approximately 8.8, 17.8, and 26.8 degrees 2θ; smectite shows up at 001 occurring at approximately 5.1 degrees 2θ. Solvating the sample with ethylene glycol brought out the presence of smectite as seen by the smectite 001 peak in diffractogram 2. As diffractogram 5 shows, heating the sample to 550 °C increased the height of the chlorite 001 peak, and caused the chlorite 002 to collapse. Illite was unaffected by treatment with glycerol, ethylene glycol, or heating to 300 °C and 550 °C in neither the Mg- or K-saturated samples.

The results of the residual shear strength test for the Discovery Park sample yielded a ϕ_r of approximately 25° (Table 2). The Atterberg limit tests yielded a LL of 55, a PL of 28 and a PI of 27, and the hydrometer test conducted in this study produced a clay fraction of 64%.

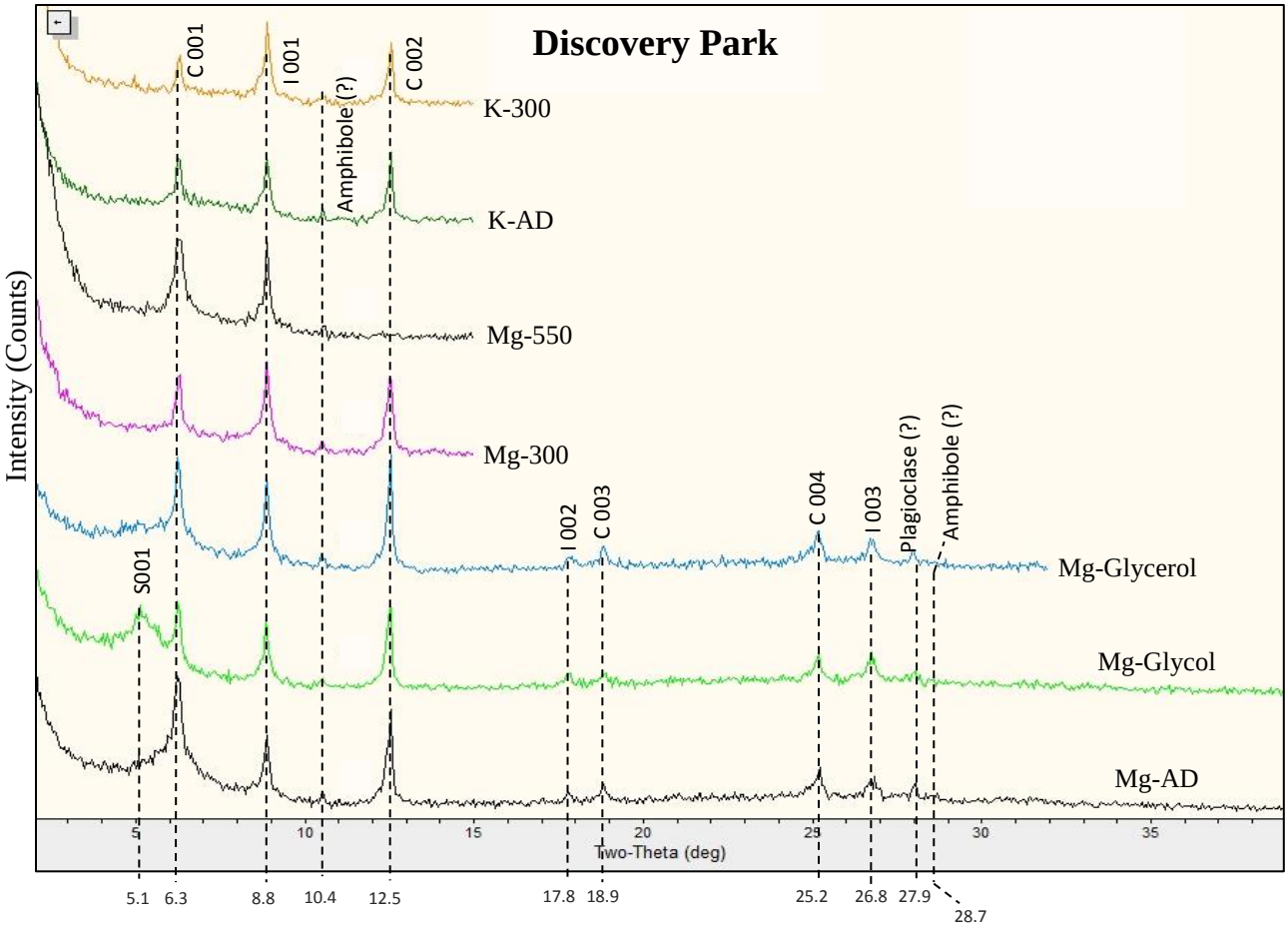

Figure 22. Diffraction patterns for the Discovery Park sample showing the changes in the magnitude of the reflectance peaks in response to the chemical and heat treatments. The patterns for each treatment are labeled as follows: Mg = magnesium chloride-saturated; K = potassium chloride-saturated; AD = air-dried; Glycol = ethylene glycol-solvated; Glycerol = glycerol-solvated; 300 = oven-heated to 300 °C; 550 = oven-heated to 550 °C. I was able to save time through the course of this study by running the Mg-Glycerol scan from 2 to 32 degrees 2θ, and the Mg-300, Mg-550, K-AD, and K-300 patterns from 2 to 15 degrees 2θ. These shorter 2θ ranges were sufficient to capture the effects of these treatments for analytical purposes.

A.5 SR-520 Shaft 7

The results of the XRD scans for the SR-520 Shaft 7 sample reflect the presence of chlorite, illite and smectite (Figure 20). The peaks labeled 001, 002, 003, 004 and 005 that respectively occur at approximately 6.3, 12.5, 18.9, 25.2 and 31.6 degrees 2θ designate chlorite; illite is indicated by peaks 001, 002 and 003 occurring at approximately 8.8, 17.8, and 26.8 degrees 2θ; smectite shows up at 001 occurring at approximately 5.1 degrees 2θ. Solvating the sample with ethylene glycol brought out the presence of smectite as seen by the smectite 001 peak in diffractogram 2. As diffractogram 5 shows, heating the sample to 550 °C increased the height of the chlorite 001 peak, and caused the chlorite 002 to collapse. Illite was unaffected by treatment with glycerol, ethylene glycol, or heating to 300 °C and 550 °C in neither the Mg- or K-saturated samples.

The results of the residual shear strength test for the SR-520 Shaft 7 sample yielded a ϕ_r of approximately 12° for the test WSDOT had previously conducted using the non-adjustable sample vessel (Table 2). The Atterberg limit tests yielded a LL of 64, a PL of 32, and a PI of 32, and the hydrometer test produced a clay fraction of 52%.

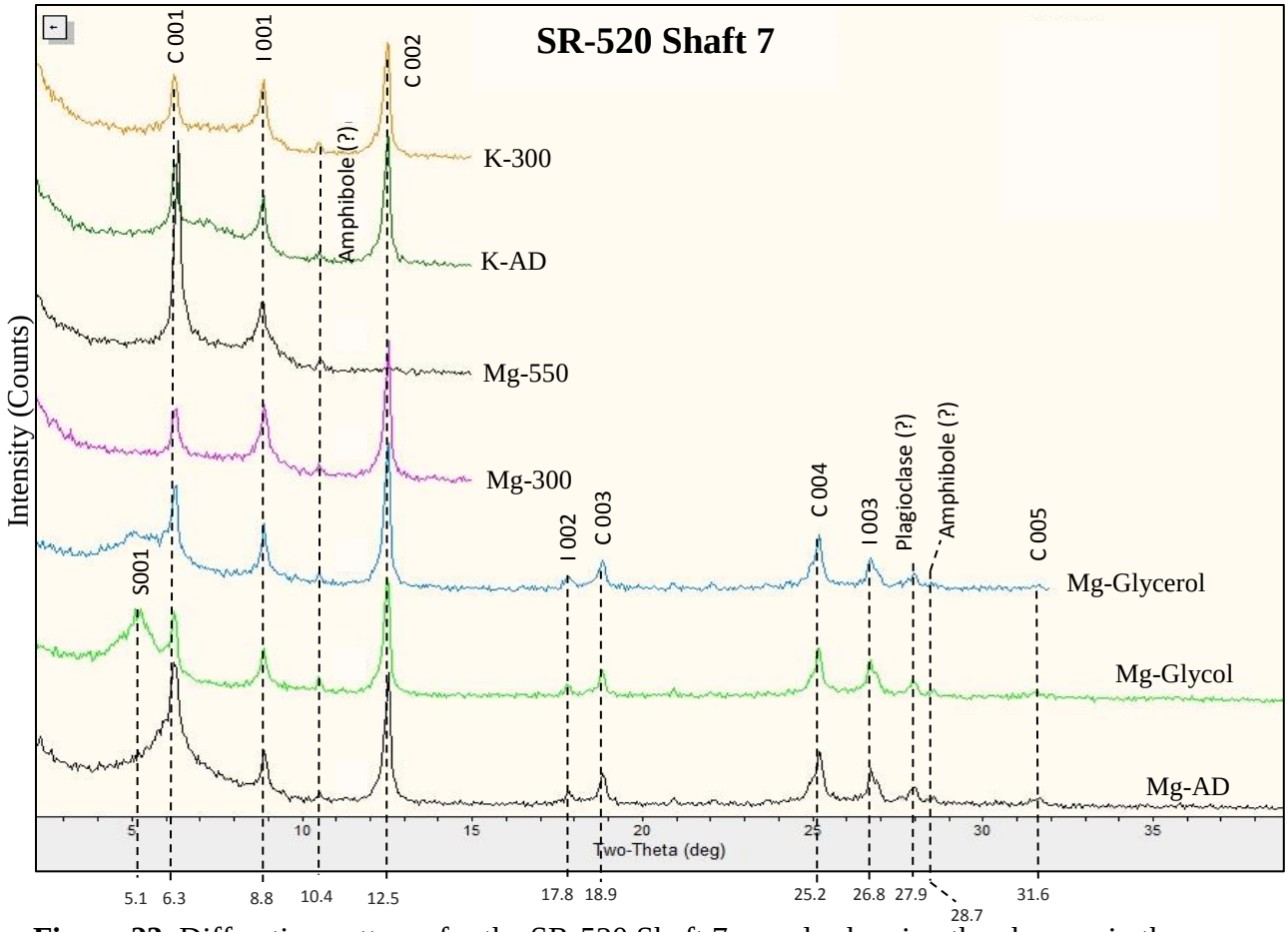

Figure 23. Diffraction patterns for the SR-520 Shaft 7 sample showing the changes in the magnitude of the reflectance peaks in response to the chemical and heat treatments. The patterns for each treatment are labeled as follows: Mg = magnesium chloride-saturated; K = potassium chloride-saturated; AD = air-dried; Glycol = ethylene glycol-solvated; Glycerol = glycerol-solvated; 300 = oven-heated to 300 °C; 550 = oven-heated to 550 °C. I was able to save time through the course of this study by running the Mg-Glycerol scan from 2 to 32 degrees 2θ, and the Mg-300, Mg-550, K-AD, and K-300 patterns from 2 to 15 degrees 2θ. These shorter 2θ ranges were sufficient to capture the effects of these treatments for analytical purposes.

A.6 SR-520 Shaft 18

The results of the XRD scans for the SR-520 Shaft 18 sample reflect the presence of chlorite, illite and smectite (Figure 21). The peaks labeled 001, 002, 003, and 004 that respectively occur at approximately 6.3, 12.5, 18.9, and 25.2 degrees 2θ designate chlorite; illite is indicated by peaks 001, 002 and 003 occurring at approximately 8.8, 17.8, and 26.8 degrees 2θ; smectite shows up at 001 occurring at approximately 5.1 degrees 2θ. Solvating the sample with ethylene glycol brought out the presence of smectite as seen by the smectite 001 peak in diffractogram 2. As diffractogram 5 shows, heating the sample to 550 °C increased the height of the chlorite 001 peak, and caused the chlorite 002 to collapse. Illite was unaffected by treatment with glycerol, ethylene glycol, or heating to 300 °C and 550 °C in neither the Mg- or K-saturated samples.

The results of the strength tests for the SR-520 Shaft 18 sample yielded a ϕ_r of approximately 17° for the test WSDOT had previously conducted using the non-adjustable sample vessel (Table 2). The Atterberg limit tests yielded a LL of 56, a PL of 25 and a PI of 31, and the hydrometer test produced a clay fraction of 40%.

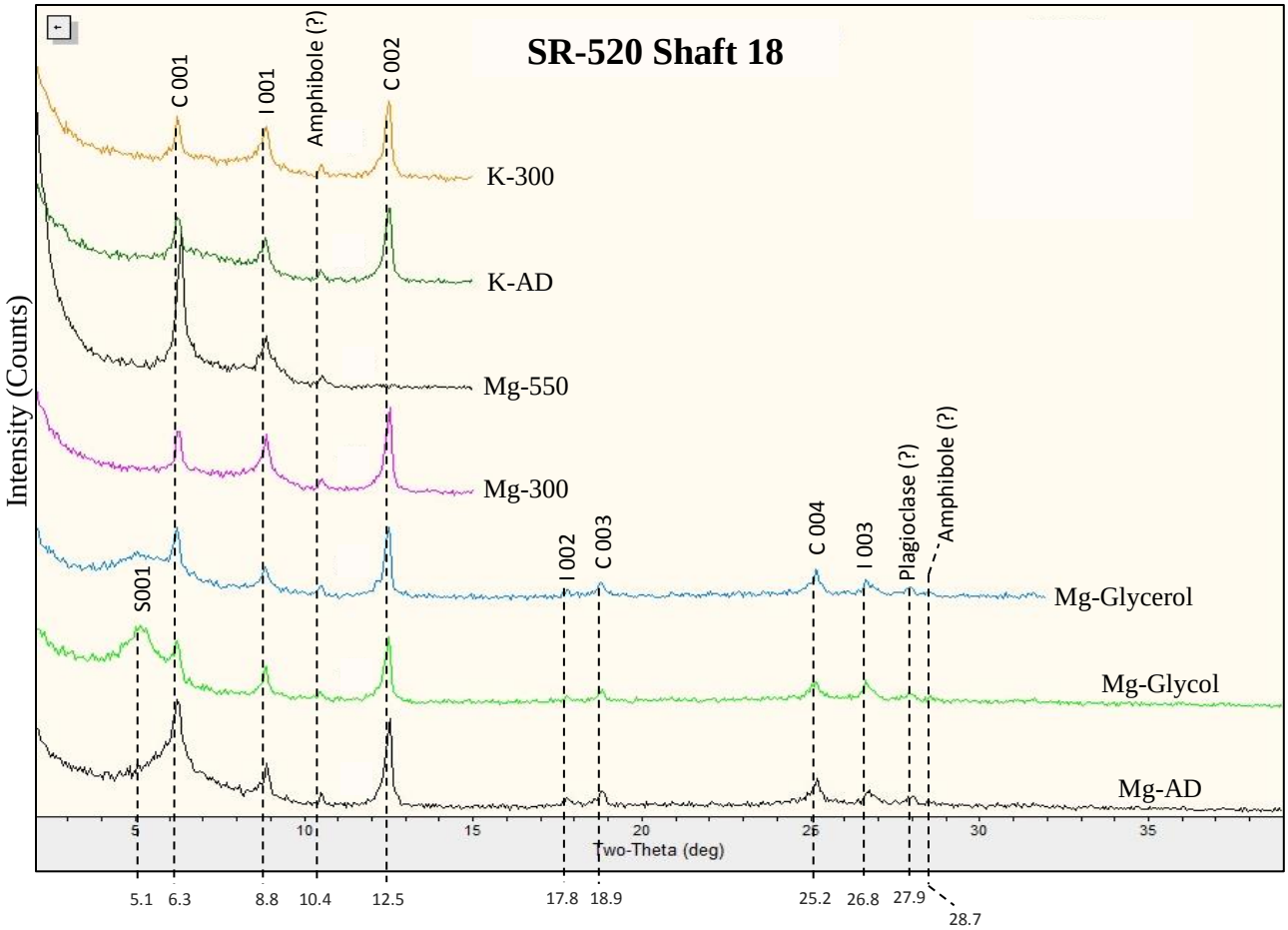

Figure 24. Diffraction patterns for the SR-520 Shaft 18 sample showing the changes in the magnitude of the reflectance peaks in response to the chemical and heat treatments. The patterns for each treatment are labeled as follows: Mg = magnesium chloride-saturated; K = potassium chloride-saturated; AD = air-dried; Glycol = ethylene glycol-solvated; Glycerol = glycerol-solvated; 300 = oven-heated to 300 °C; 550 = oven-heated to 550 °C. I was able to save time through the course of this study by running the Mg-Glycerol scan from 2 to 32 degrees 2θ, and the Mg-300, Mg-550, K-AD, and K-300 patterns from 2 to 15 degrees 2θ. These shorter 2θ ranges were sufficient to capture the effects of these treatments for analytical purposes.

A.7 SR-520 Shaft 21

The results of the XRD scans for the SR-520 Shaft 21 sample reflect the presence of chlorite, illite and smectite (Figure 22). The peaks labeled 001, 002, 003, 004 and 005 that respectively occur at approximately 6.3, 12.5, 18.9, 25.2 and 31.6 degrees 2θ designate chlorite; illite is indicated by peaks 001, 002 and 003 occurring at approximately 8.8, 17.8, and 26.8 degrees 2θ; smectite shows up at 001 occurring at approximately 5.1 degrees 2θ. Solvating the sample with ethylene glycol brought out the presence of smectite as seen by the smectite 001 peak in diffractogram 2. As diffractogram 5 shows, heating the sample to 550 °C increased the height of the chlorite 001 peak, and caused the chlorite 002 to collapse. Illite was unaffected by treatment with glycerol, ethylene glycol, or heating to 300 °C and 550 °C in neither the Mg- or K-saturated samples.

The results of the strength tests for the SR-520 Shaft 21 sample yielded a ϕ_r of approximately 29° for the test WSDOT had previously conducted using the non-adjustable sample vessel (Table 2). The Atterberg limit tests yielded a LL of 39, a PL of 26 and a PI of 13, and the hydrometer test produced a clay fraction of 17%.

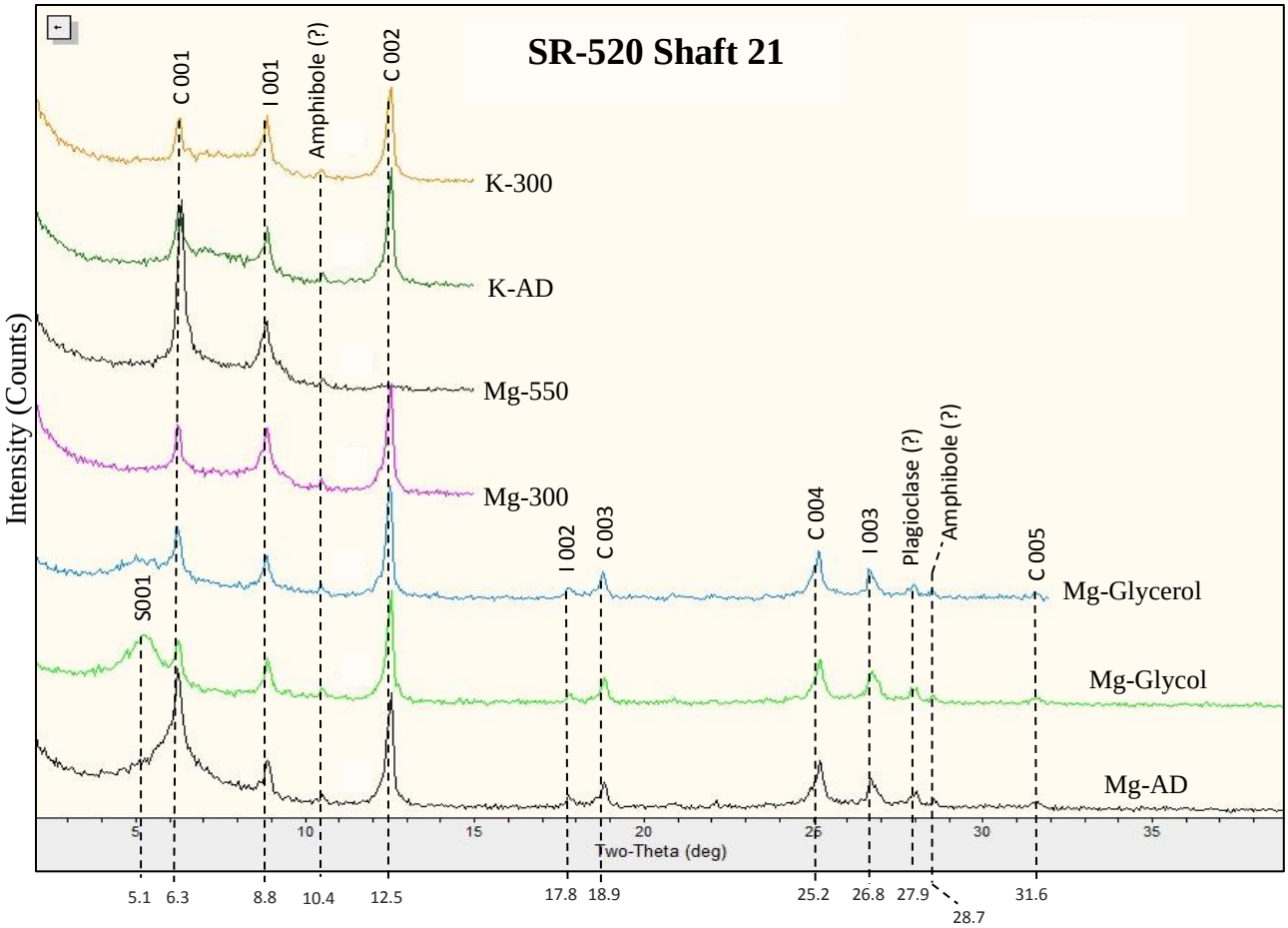

Figure 25. Diffraction patterns for the SR-520 Shaft 21 sample showing the changes in the magnitude of the reflectance peaks in response to the chemical and heat treatments. The patterns for each treatment are labeled as follows: Mg = magnesium chloride-saturated; K = potassium chloride-saturated; AD = air-dried; Glycol = ethylene glycol-solvated; Glycerol = glycerol-solvated; 300 = oven-heated to 300 °C; 550 = oven-heated to 550 °C. I was able to save time through the course of this study by running the Mg-Glycerol scan from 2 to 32 degrees 2θ, and the Mg-300, Mg-550, K-AD, and K-300 patterns from 2 to 15 degrees 2θ. These shorter 2θ ranges were sufficient to capture the effects of these treatments for analytical purposes.

A.8 Klickitat Drive

The results of the XRD scans for the Klickitat Drive sample reflect the presence of chlorite, illite and smectite (Figure 23). The peaks labeled 001, 002, 003, 004 and 005 that respectively occur at approximately 6.3, 12.5, 18.9, 25.2 and 31.6 degrees 2θ designate chlorite; illite is indicated by peaks 001, 002 and 003 occurring at approximately 8.8, 17.8, and 26.8 degrees 2θ; smectite shows up at 001 occurring at approximately 5.1 degrees 2θ. Solvating the sample with ethylene glycol brought out the presence of smectite as seen by the smectite 001 peak in diffractogram 2. As diffractogram 5 shows, heating the sample to 550 °C increased the height of the chlorite 001 peak, and caused the chlorite 002 to collapse. Illite was unaffected by treatment with glycerol, ethylene glycol, or heating to 300 °C and 550 °C in neither the Mg- or K-saturated samples.

The results of the residual shear strength tests for the Klickitat Drive sample yielded a ϕ_r of approximately 28° for the test WSDOT had previously conducted with the non-adjustable sample vessel, and approximately 31° for the test I conducted in this study using the adjustable vessel (Table 2). The Atterberg limit tests yielded a LL of 33, a PL of 27 and a PI of 6 (Table 2 and Figure 9). The hydrometer test produced a clay fraction of 10%.

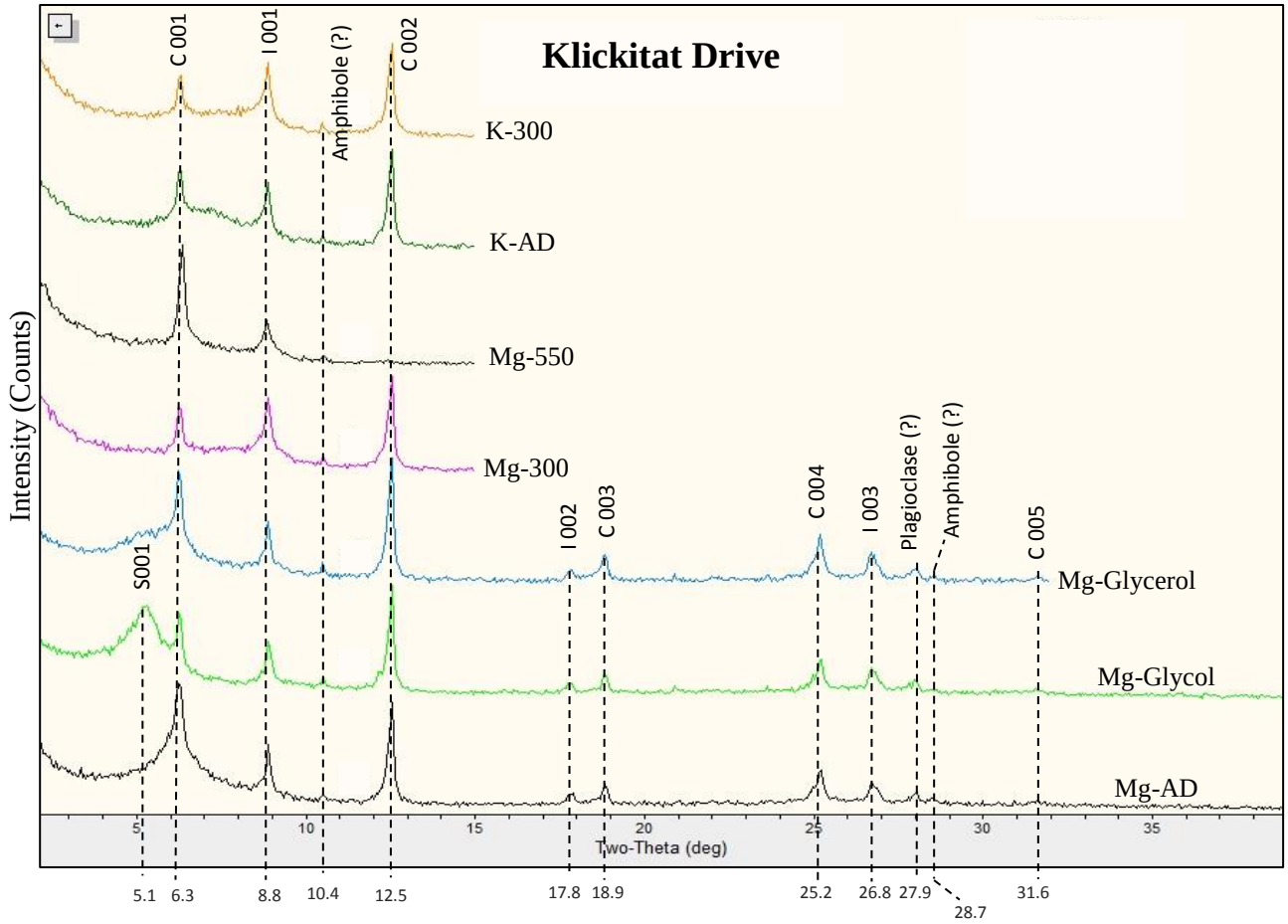

Figure 26. Diffraction patterns for the Klickitat Drive sample showing the changes in the magnitude of the reflectance peaks in response to the chemical and heat treatments. The patterns for each treatment are labeled as follows: Mg = magnesium chloride-saturated; K = potassium chloride-saturated; AD = air-dried; Glycol = ethylene glycol-solvated; Glycerol = glycerol-solvated; 300 = oven-heated to 300 °C; 550 = oven-heated to 550 °C. I was able to save time through the course of this study by running the Mg-Glycerol scan from 2 to 32 degrees 2θ, and the Mg-300, Mg-550, K-AD, and K-300 patterns from 2 to 15 degrees 2θ. These shorter 2θ ranges were sufficient to capture the effects of these treatments for analytical purposes.